4 HALCA Constraints

HALCA has a number of constraints which may make it impossible for the spacecraft to observe a given source under certain conditions. An understanding of the spacecraft constraints enables the proposer to understand what type of observations are feasible and what time scales are appropriate for monitoring observations.

4.1 Sun

Before the launch of HALCA, it was expected that HALCA could not observe sources within a sun angle (SA) of 70° where the sun angle is defined to be the angle between the source and the sun. This constraint arises from the fact that the solar panels must be fully illuminated by the Sun to generate sufficient power for scientific observations. When a source is within 70° of the Sun the main antenna shadows the solar panels; they are therefore under-illuminated and cannot provide the required solar power. However, in-orbit experience has shown that for certain sun angles beyond 70° that the spacecraft experiences larger torques than those predicted before launch. These torques cause the reaction wheels of the attitude control subsystem to absorb more angular momentum throughout an orbit than the maximum design value (The reaction wheels are unloaded at each perigee by magnetic torquing using the Earth's magnetic field). Therefore, at the present time, HALCA is unable to observe sources within the sun angle ranges 0–80°and 110–145°. The impact of the present solar constraints are described more fully in §4.9.

4.2 Moon

HALCA cannot observe sources occulted by the moon.

4.3 Earth

Like ground radio telescopes, HALCA cannot observe sources occulted by the Earth. Unlike ground radio telescopes, which are fixed to the Earth, the varying altitude of HALCA means that the fraction of the sky occupied by the Earth varies. At the closest approach of the spacecraft to the Earth (perigee), the Earth occupies 30% of the celestial sphere, whereas at the furthest point from the Earth (apogee) the Earth only occupies 1.3% of the celestial sphere. Thus, this constraint is less severe for HALCA than it is for a ground radio telescope.

4.4 Eclipse

HALCA cannot observe when the Sun is occulted by the Earth or the Moon. When this happens, the spacecraft has to use its batteries to power the spacecraft. Scientific observations are not possible during eclipse because they would cause too large a drain on the batteries. Furthermore, after each eclipse the batteries are re-charged and this battery re-charge time is roughly equal to the eclipse length. During the battery re-charge time it is also not possible to undertake scientific observations. Figure 3 shows HALCA eclipse history from 1-Oct-98 to 31-Dec-99. As can be seen, in this period there are two seasons of no eclipses, a long season (25-Jan-99 to end of second AO period) of relatively short eclipses lasting $\approx$ 20-40 minutes and a relatively short season (9-Oct-98 to 3-Nov-98) of long eclipses lasting at most$\approx$ 90 minutes. During this short season of long eclipses no scientific observations will be undertaken.

Eclipses produce gaps in (u,v) coverages that stay fixed from orbit to orbit on the timescale of a typical observation.

4.5 Tracking Network

HALCA is supported by a 5-station tracking network (see §6 for more details). The high VLBI data rate (128 Mbps) requires that the VLBI data must be down-linked in real time. Therefore it is impossible for the satellite to observe if it is not above the minimum elevation limit (typically 5°) of any tracking station.

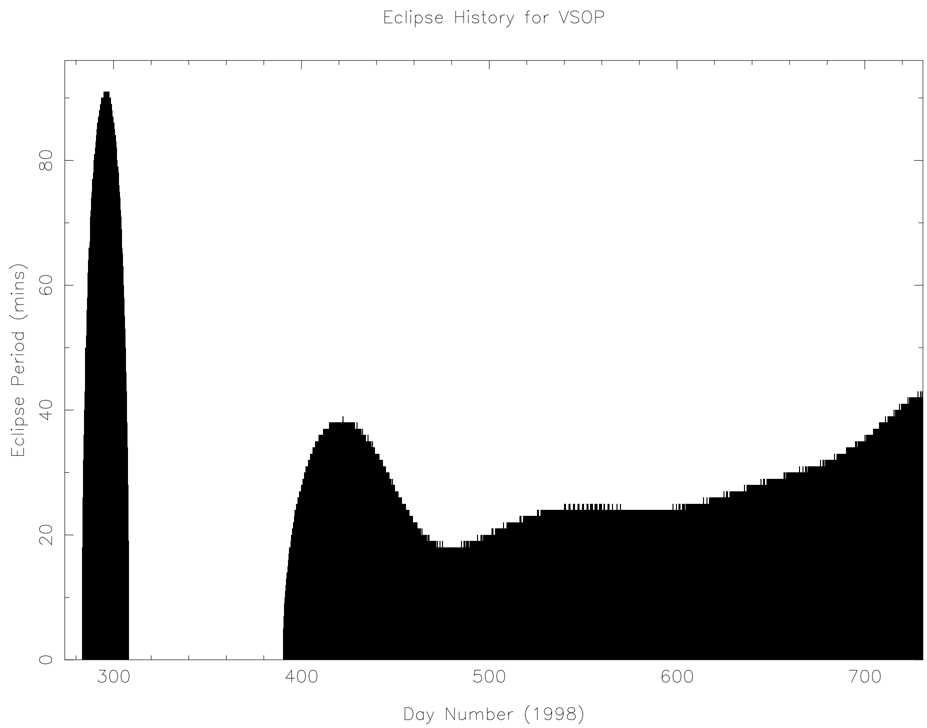

Figure 3: HALCA eclipse history (1-Oct-98 to 31-Dec-99).

In addition, the satellite depends upon contact with a ground tracking station for its local oscillator phase reference.

4.6 Spacecraft Telemetry Horizon Mask

Even if all of the above constraints are met it still may be impossible to observe. HALCA has only one telemetry antenna to transmit the VLBI data to the tracking stations. The telemetry antenna is on a boom attached to the opposite side of the spacecraft main body from the main (8m) antenna. This telemetry antenna itself has a limited field of view, so it cannot communicate with a tracking station if, from the perspective of the telemetry antenna, the tracking station lies within $\approx 70°$of the source direction. Thus, in order to communicate with a tracking station, the spacecraft must be above the minimum elevation limit of the tracking station and the tracking station must lie within the field of view of the telemetry antenna.

4.7 Slew Time and Settling

When changing sources, the VSOP satellite can slew at a rate of $2.25°$ min^{-1}. However, slewing is a two-stage process which means that the total angle the spacecraft slews through is greater than or equal to the angle between the two sources. The satellite first slews around the spacecraft-Sun axis followed by a slew about the solar-panel axis. Thus, even under optimum conditions, it takes 80 minutes to slew $180°$. Furthermore, once the slew is completed it takes ≈ 3 minutes for the antenna to settle. In general, proposers do not need to worry about spacecraft slewing as this is taken care of during the scheduling of HALCA.

4.8 On-board Command Memory

Once a day (except for Sunday) HALCA receives a new command sequence from the Kagoshima Space Center (see Table 5). This command sequence is composed of at most 256 commands, some of which are devoted to scientific activities. One command is required for each of the following scientific activities: (1) to turn the noise diodes on or off, (2) to change frequency band and/or LO settings, and (3) to change source. Thus there is a trade-off to be made between how frequently to change source, how frequently to change observing band and/or LO settings and how frequently to measure the system temperature. Furthermore it is only possible to observe a maximum of four sources in each command sequence. Although it takes only one command to change source, each source itself requires additional information that is used primarily by the star sensors in the attitude control subsystem. The one exception to the four sources rule is for sources separated by $< 3°$. In this case it is possible to change sources using the attitude control subsystem, so that the new source is represented internally as the old source with a pointing offset. Although this method may appear attractive for phase-referencing observations, it should be remembered that the settling time of the antenna needs to be taken into account and that the fractional baseline error is much higher for spacecraft-Earth than for the Earth-Earth baselines. Phase-referencing observations will not be possible at 5 GHz, and will be marginal at 1.6 GHz. Proposers who wish to use this method of changing sources should consult the VSOG by e-mail (vsog@vsop.isas.ac.jp) as to its technical feasibility. Before launch, it expected that ≈200 commands would be used for system temperature measurements. However, after launch, it was discovered that the autonomous heater control electronics has some anomalies. Since then many of these commands that were to be used to measure the system temperature have been replaced by heater control commands. Thus, instead of measuring the system temperature during a VLBI experiment, it is now measured before or after the experiment (see §12 for more details).

4.9 Impact of the Solar Constraints

Before launch it was expected that HALCA would be unable to observe sources within 70°of the sun. After launch it was discovered that the range of allowed sun angles was not the 70°–180°but rather 80°–110° and 145°–180°. Since these constraints refer to the sun it is easiest to understand them in terms of the source's ecliptic latitude (β) and longitude (λ) which are related the source's right ascension (α) and declination (δ) as follows:

$$\boxed{\beta = \sin^{-1}(\cos\epsilon\sin\delta - \sin\epsilon\sin\alpha\cos\delta)} \tag{1}$$

$$\boxed{\lambda = \tan^{-1}(\tfrac{\cos\epsilon\sin\alpha+\sin\epsilon\tan\delta}{\cos\alpha})} \tag{2}$$

where ϵ = obliquity of the ecliptic ($\approx 23.5°$)

First of all, we will examine the old sun angle constraint of 70°. Sources with $|\beta| > 70°$are never within 70°of the sun so were not affected by this constraint. For sources with $|\beta| < 70°$, during a year the source is unobservable for a period ($\Delta t_{\rm unobs}$) of time given by:

$$\boxed{\Delta t_{\rm unobs} = (365/180)\cos^{-1}(\tfrac{\cos 70}{\cos\beta})\ \text{days}} \tag{3}$$

$\Delta t_{\rm unobs}$ is a maximum for sources that lie in the ecliptic plane and this maximum value is 141 days (4.7 months).

For the present solar constraints what happens again depends on the ecliptic latitude of the source:

- $|\beta| < 35°$: source can be observed in three windows a year.
- $35° < |\beta| < 70°$: source can be observed in two windows a year.
- $70° < |\beta| < 80°$: source can be observed for a single window a year.
- $|\beta| > 80$: source can be observed all the time.

Table 3 shows how large these observing windows are as a function of β. In this table we define a time co-ordinate in days such that the sun and the source have the same ecliptic longitude at t = 0 days. A source with a given β has a sun angle (SA) of 80°, 110°, and 145°at t_{80}, t_{110}, and t_{145} respectively. As can be seen a source with a given β has a certain SA twice a year (or not at all if $|\beta| >$ SA for SA < 90°or if $|\beta| >$ (180°-SA) for SA > 90°). Observing windows occur when 80°<= SA <= 110°and when 145°<= SA <= 180°. The first window lasts Δt_{80-110} days and the second window lasts $\Delta t_{145-180}$ days. There can either be 1 or 2 occurrences of the first window in a year depending on whether $|\beta|$ is less or greater than 70°. Table 3 also shows the number of observing windows per year ($n_{\rm windows}$) and the total number of days a year a source with a given β can be observed both with the present solar constraints ($\Delta t_{\rm present}$) and the old solar constraints ($\Delta t_{\rm old}$).

Table 3: Sun Angle Observing Windows

$\beta(°)$	t_{80}	t_{110}	t_{145}	n × Δt_{80-110}	n × $\Delta t_{145-180}$	$n_{\rm windows}$	$\Delta t_{\rm present}$	$\Delta t_{\rm old}$
00	81, 284	112, 253	147, 218	2×30	1×71	3	132	224
10	81, 284	112, 253	148, 219	2×31	1×68	3	130	224
20	81, 284	113, 252	153, 212	2×32	1×60	3	124	226
30	80, 285	115, 250	163, 202	2×35	1×38	3	109	230
40	78, 287	118, 247	-	2×40	-	2	80	236
50	75, 290	124, 241	-	2×49	-	2	97	248
60	71, 294	135, 230	-	2×64	-	2	129	270
70	60, 305	-	-	1×122	-	2	245	365
80	-	-	-	1×365	-	1	365	365
90	-	-	-	1×365	-	1	365	365

These new solar solar constraints have a serious impact on monitoring observations since in general it is not possible to continuously observe a source with HALCA. Therefore, monitoring observations will have to take place either within a single observing window (which as can be seen can last for ≈ 30 to ≈ 60 days) or will have to span multiple observing windows. In the case of 3 windows a year ($|\beta| < 35°$) these windows are roughly centered 3-months apart. In the case of 2 windows a year ($35° < |\beta| < 70°$), these windows are roughly centered 6-months apart. Furthermore, there is no guarantee that good (u,v) coverage can be obtained during a particular observing window since other constraints may not be met at this time. For example, the source may lie in the orbit plane for the duration of a window which gives only one-dimensional (u,v) coverage.

It should be noted that the solar constraints described here are the present HALCA solar constraints. It is possible that these constraints might be relaxed during AO2 observations. If they are and this is known before the AO2 proposal deadline then this information will be announced in the VSOP newsletter. Proposers are allowed to propose observations that lie outside the present solar constraints. However, if it turns that the present solar constraints are not relaxed then it will not be possible to undertake any observations that lie outside these constraints.

5 HALCA Orbit

Space VLBI is simply ground VLBI with, in the case of the VSOP mission, an additional antenna in space. Since the science that can be produced by the VSOP mission is intimately tied to HALCA orbit, proposers need to be aware of the basic properties of orbits and how they change with time.

Table 4: Nominal HALCA Orbital Elements (Defined at 0 UT on 24-February-1998)

Keplerian Orbital Element	Value
a (semi-major axis)	17,367.457 km
e (eccentricity)	0.6015
i (inclination)	31.46°
Ω (right ascension of the ascending node)	16.0435°
ω (argument of perigee)	106.7552°
M (mean anomaly)	66.2098°
Derived Parameters	
Orbital period	6.33 hours
Apogee height	21,436 km
Perigee height	543 km
Perigee velocity	2.39 km/s
Apogee velocity	9.61 km/s

Note: These orbital elements are those that should be used with simulation software for simulations that cover the second AO period.

5.1 Definition of the Orbital Elements

To a good approximation, an orbit bound to the Earth is an ellipse with the Earth at one of the foci. It is convenient to refer to the orbit by the properties of this ellipse – the so-called six Keplerian orbital elements. Five of the six elements refer to the properties of the orbit ellipse and its orientation in space. The sixth element determines the location of the spacecraft on this ellipse. These elements, which are defined at a certain epoch, are:

a: Semi-major axis. The spacecraft orbital period, T, is related to the semi-major axis as follows $\mathrm{T} = 2.76\ (a/10^4\,\mathrm{km})^{3/2}$ hours.

e: Eccentricity. The distance of the spacecraft from the center of the Earth at the closest approach to the Earth (perigee) is given by $a(1-e)$. The distance of spacecraft at furthest point from the center of the Earth in its orbit (apogee) is given by $a(1+e)$. To calculate the spacecraft height above the surface of the Earth at either perigee or apogee it is necessary to subtract the radius of the Earth from the previous expressions. The orbit semi-minor axis, b, is given by $a\sqrt{1-e^2}$.

i: Inclination. This is defined as $\cos^{-1}(L_z)$, where L_z is the component of the orbit unit angular momentum vector that lies along the Earth's rotation axis. For orbits that lie in the celestial equator (equatorial orbits), $L_z = 1$, and hence $i = 0°$. For orbits perpendicular to the celestial equator (polar orbits), $L_z = 0$ and hence $i = 90°$. HALCA's orbit is inclined 31° to the equator.

Ω: Right ascension (or longitude) of the ascending node. Except for equatorial orbits, a spacecraft crosses the celestial equator twice every orbit: once when it is heading north and once when it is heading south. Ω is the right ascension of the spacecraft when it crosses the celestial equator heading north. This point is known as the ascending node. Like right ascension, Ω is usually measured in hours, but in some circumstances degrees is a more appropriate unit.

ω: Argument of perigee. This is defined as the angle in the orbital plane between the ascending node and perigee as measured from the center of the Earth. When ω is between 0° and 180° the perigee is in the northern hemisphere. Otherwise it is in the southern hemisphere.

M: Mean anomaly. Due to the conservation of angular momentum, the spacecraft moves at a non-uniform rate around the orbit ellipse. The angle between the spacecraft and perigee, as measured from the center of the Earth, is called the true anomaly. However it is convenient to work with another angle called the mean anomaly. If this is measured in degrees, the ratio M/360 is equal to the ratio of the time elapsed since the spacecraft last passed through perigee to the spacecraft orbital period. Thus, for a spacecraft at perigee, $M = 0°$, and for a spacecraft at apogee, $M = 180°$. For a spacecraft in a circular orbit ($e = 0$) the mean anomaly and the true anomaly are the same.

The HALCA orbital elements are shown in Table 4.

5.2 Orbit Normal and (u,v) Coverages

The orientation of the orbital plane in space and the orientation of the orbit semi-major axis within the orbital plane control the type of (u,v) coverage that can be obtained for a given source, provided that the spacecraft constraints can be met. The orbit normal, which lies in the northern hemisphere, and the orbit anti-normal, which lies in the southern hemisphere, define directions along which the highest two-dimensional resolution observations will be obtained i.e., those observations for which the synthesized beam area is a minimum. The celestial coordinates (α, δ) of the orbit normal and the orbit anti-normal are ($\Omega-$6h, $90°-i$) and ($\Omega+$6h, $i-90°$) respectively. For sources that lie in the orbital plane, that is 90° from the orbit normal, approximately linear (u,v) coverages are obtained.

Figure 4 shows an example of how the (u,v) coverage varies as a function of α and δ at a particular epoch. The case where the source is in the orbit plane can be clearly seen, since this is where linear (u,v) coverage is obtained. The large regions with (u,v) coverages that have no space-ground baselines are due to the solar constraint that HALCA cannot observe in the range of sun angles 0°–70°and 110°–145°. These regions move with the sun across the sky during the year. More examples of how the (u,v) coverages vary during AO phase 2 observations are shown in Appendix D. AO phase 2 observations nominally cover a 12 month observing period beginning in January 1999 and ending in December 1999. However, some observations may be scheduled as early as October 1998 if better (u,v) coverage can be obtained for the source at an earlier epoch compared to the nominal AO phase 2 period.

At apogee, for a source that lies along the orbit normal direction, the projected baseline lengths range from about 23,000 km to 33,000 km depending on the location of the ground radio telescopes with respect to the spacecraft. Since this lower limit exceeds the maximum baseline that can be obtained with ground-based VLBI arrays ($\approx$ 10,000 km) it inevitably follows that there will be large holes in the (u,v) plane for sources observed along or near the orbit normal (or anti-normal) direction. However, for sources that lie away from the orbit normal direction, the size of these (u,v) holes can be minimized by projection effects. Proposers who want to request specfic observing dates for either single epoch experiments or monitoring experiments can do so in item(10), the 'Additional notes to the scheduler' box on the Cover Sheets.

5.3 Precession of the Orbital Elements

Due to the oblateness of the Earth, the orbital elements ω and Ω precess, which has a significant impact on the (u,v) coverage that can be obtained for a given source as a function of time. These precession rates are given by:

$$\boxed{\dot{\Omega} = -752\frac{\cos i}{(1-e^2)^2}\left(\frac{a}{10^4\,km}\right)^{-\frac{7}{2}}\ ^{\circ}\,\mathrm{yr}^{-1}} \qquad (4)$$

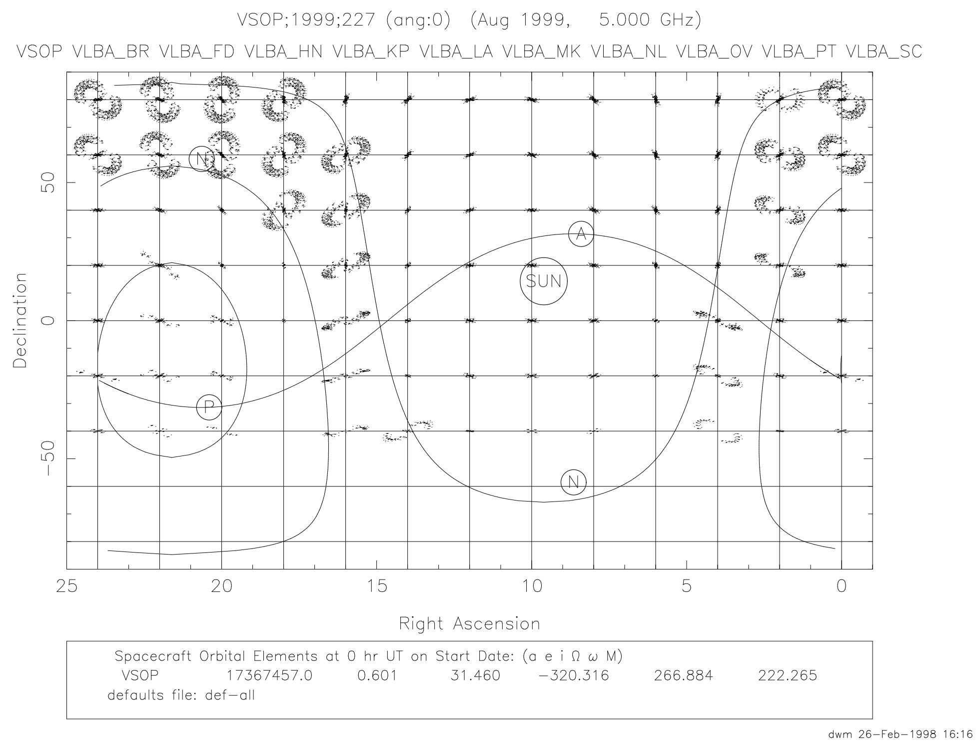

Figure 4: All-Sky (u,v) plot for HALCA with the VLBA on 15 Aug 1999.

$$\boxed{\dot{\omega} = -\frac{1}{2}\left(\frac{5\cos^2 i - 1}{\cos i}\right)\dot{\Omega}} \tag{5}$$

For the HALCA orbit, $\dot{\Omega} = -228^\circ\,\mathrm{yr}^{-1}$ and $\dot{\omega} = +353^\circ\,\mathrm{yr}^{-1}$.

5.3.1 Impact of Ω Precession

One major consequence of the Ω precession is that the direction of the orbit normal changes with time, and hence the directions in the sky for which the best (u,v) coverages are obtained also change with time. Figure 5 shows an example of how for a particular source, 3C345 (B1641+399), the (u,v) coverage varies as a function of time. As can be seen, the (u,v) coverage changes quite dramatically with time.

Plots like those shown in Figure 5 are particularly useful in planning monitoring observations (see §13 on simulation software).

5.3.2 Impact of ω Precession

A major consequence of the ω precession is that the amount of tracking available for HALCA, and hence the amount of space VLBI data that can be obtained during an observation, is a function of ω, and hence the epoch of the observation. The reason for this is that four of the five tracking stations are located in the northern hemisphere (see Table 5). Hence more space VLBI data is obtained when the apogee of the orbit is in the northern hemisphere ($180^\circ < \omega < 360^\circ$) compared to when the apogee is in the south ($0^\circ < \omega < 180^\circ$). See §6 for more details on the tracking network. The relationship between ω and day of the year for 1999 (DOY_{1999}) is as follows:

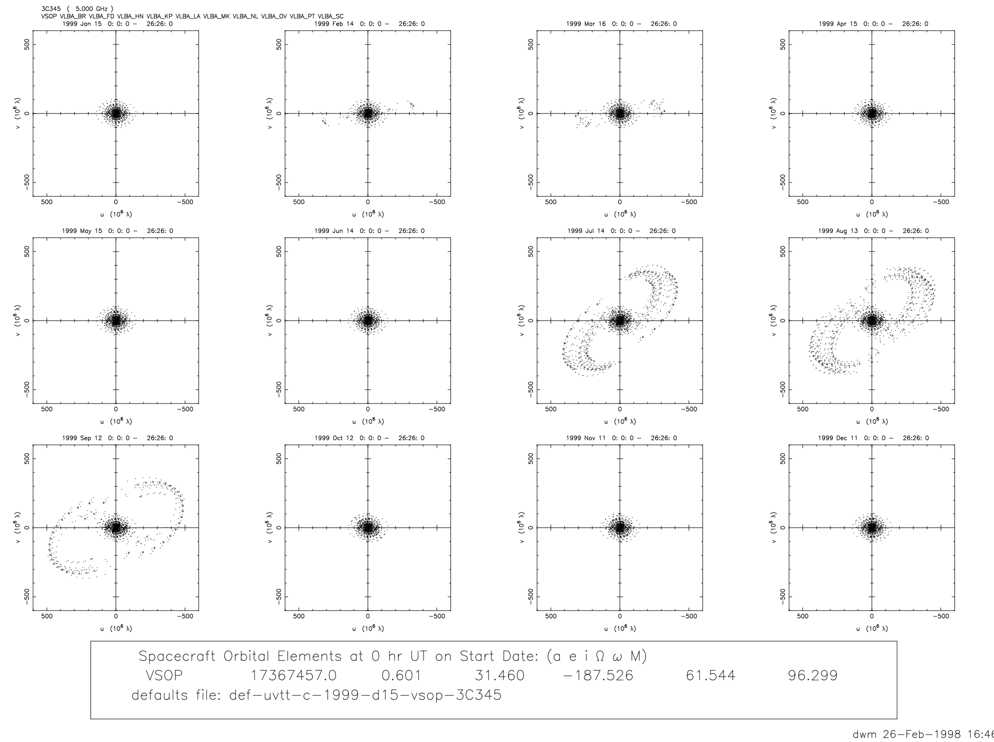

Figure 5: Example (u,v) plot as a function of time. (u,v) coverages for a 22-hour observation of 3C345 with HALCA and the VLBA, starting at the top left on 15 Jan 1999 and going from left to right with a (u,v) coverage produced once a month for a one year period.

$$\boxed{\mathrm{DOY}_{1999} \approx -45.6 + 0.9918\,\omega} \tag{6}$$

Thus, the best tracking during the second AO period is when $\omega = 270°$and hence from the above equation when the DOY_{1999} is 222 (10-Aug-1999). Similarly, the poorest tracking occurs when $\omega = 90°$and hence $DOY_{1999} = 44$ (13-Feb-1999).

Furthermore there is an interaction between the field of view of the VSOP spacecraft telemetry antenna and ω that limits the amount of tracking that is available for certain sources under certain conditions. For example, when apogee is in the northern hemisphere it is difficult to observe far southern sources at or near apogee, since under these conditions the telemetry antenna points away from the Earth and cannot communicate with a tracking station (see §4.6).

Proposers should use the orbit listed in Table 4 when planning what observations are feasible. During the scheduling process, any differences between the nominal and actual satellite orbit will be taken into account when scheduling a particular observation.

6 HALCA Tracking Network

Unlike ground VLBI radio telescopes, for which the hydrogen maser reference signal and VLBI data recorder are typically located close to the antenna, for HALCA these facilities are located at a tracking station many thousands of kilometers from the spacecraft. Two types of tracking stations support HALCA: (1) A single commanding station (S-band) at Kagoshima, Japan, and (2) Five VLBI data acquisition and phase transfer stations (K_u-band). In other parts of this guide the VLBI data acquisition and phase transfer stations are simply called tracking stations. Table 5 lists the location of these stations.

Table 5: HALCA Tracking Network

Location	Code	Latitude	Longitude	Recorder	Agency
Commanding Station (S-band)					
Kagoshima, Japan	-	31°N	131°E	—	ISAS
Tracking Stations (K_u-band) – VLBI Data Acquisition and Phase Transfer					
Usuda, Japan	UZ	36°N	138°E	VLBA/VSOP/S2	ISAS
Goldstone, California, USA (DSS-23)	GZ	35°N	116°W	VLBA/S2	NASA/JPL
Robledo, Spain (DSS-53)	RZ	40°N	4°W	VLBA/S2	NASA/JPL
Tidbinbilla, Australia (DSS-33)	TZ	35°S	149°E	VLBA/S2	NASA/JPL
Green Bank, West Virginia, USA	NZ	38°N	80°W	VLBA/S2	NRAO

HALCA is commanded once a day (except for Sunday) from Kagoshima and the international network of 5 VLBI data acquisition tracking stations collect the VLBI data throughout each day. It is important to note that 4 of these 5 VLBI data acquisition tracking stations are in the northern hemisphere. Depending on the time-variable argument of perigee (ω) of the VSOP spacecraft orbit (see §5.3.2), the amount of time that HALCA is above the elevation limits of the VLBI data acquisition tracking stations varies from 55% of the time (for the worst case when $\omega = 90°$) to 85% of the time (for the best case when $\omega = 270°$). The VLBI data acquisition tracking stations record the VLBI data on either VLBA or S2 recorders, with the exception of Usuda which can also record the data on a VSOP terminal (VSOP-T) recorder. After the completion of an observation, the VLBI tapes are shipped to the appropriate correlator. Various auxiliary data are sent to the VSOG, which creates various auxiliary files and sends them to the correlator. These files are needed both for correlation and subsequent data analysis. The VSOG decides which VLBI data acquisition tracking stations track the spacecraft.

7 Ground Radio Telescopes

HALCA is a single element in a VLBI array. Without ground radio telescopes to co-observe with the satellite it is unable to perform its mission. Discussions among the directors of the world's ground observatories, under the auspices of the Global VLBI Working Group (GVWG), have resulted in the forward commitment of observing time, as shown in Table 6, to space VLBI. In order to facilitate greater scheduling efficiency, some of the EVN telescopes may be scheduled preferentially at certain observing bands. For example, the Lovell telescope at Jodrell bank has committed to observe 30% of all space VLBI observations at 1.6 GHz. Ground observatories which are not fully dedicated to VLBI, such as the EVN and ATNF telescopes (ATCA and Mopra), prefer time to be allocated in blocks. It should also be noted that some observatories have especially high program pressure at certain times of year (e.g., Effelsberg during night time in May through July when the Galactic Center observations may take precedence). For each telescope, Table 6 also shows the telescope diameter, the system equivalent flux densities (SEFDs) at 1.6 and 5 GHz, the VLBI recording system (or systems), and the two letter code used to refer to an individual telescope. For comparison purposes the SEFDs for HALCA are shown at the bottom of this table. The system temperatures are the current best estimates and are subject to change. The percentage time commitment is the percentage of the number of hours in the year that the particular telescope has committed to space VLBI observations. During AO2 observations the VSOP mission may have to share observing time with the Russian RadioAstron mission, if RadioAstron is operational at that time.

Table 6: Participating Ground Radio Telescopes and VLBI Networks

GRT/Network	Code[1]	Location	Diam. (m)	SEFD (Jy)[2] 1.6 GHz	5 GHz	Recorder	Time[3]
Arecibo	AR	Puerto Rico	305	2.5	3.5	S2,VLBA[8]	4%
ATCA (Narrabri)	AT	Australia	6x22	60	80	S2	~10%
Ceduna	CD	Australia	30	—	500	S2	~4%
EVN:	EVN	Europe/Asia					
Cambridge[4]	CM	UK	32	212	136	VLBA[7], MkIV[6]	~4%
Effelsberg	EB	Germany	100	19	20	VLBA, MkIV	11%
Jodrell (Lovell)	JB	UK	76	44	—	VLBA, MkIV[6]	~5%
Jodrell (Mk II)	JB	UK	26	—	320	VLBA, MkIV[6]	10%
Medicina	MC	Italy	32	582	296	MkIV	20%
Noto	NT	Italy	32	784	260	VLBA[7], S2	15%
Onsala	ON	Sweden	25	390	600	MkIV	20%
Shanghai	SH	China	25	1088	520	VLBA[7], S2	25%
Torun	TR	Poland	32	200	220	VLBA[7], S2	15%
WSRT	WB	Netherlands	14x25	40	90	MkIV	15%
Goldstone	GO	USA	70	49	—	MkIV	7%
Green Bank (140′)[5]	GB	USA	43	80	120	VLBA, S2	~7%
Hartebeesthoek	HH	South Africa	26	370	680	S2	~10%
Hobart	HO	Australia	26	1300	1300	S2	10%
Mopra	MP	Australia	22	350	450	S2	25%
Robledo	RO	Spain	70	49	—	MkIV	7%
Tidbinbilla	TI	Australia	70	49	—	MkIV, S2	7%
Usuda	UD	Japan	64	69	69	VSOP-T, S2	~7%
VLA-27	Y	USA	27x25	14	14	VLBA	<3%
VLBA:	VLBA	USA					
Brewster	BR	USA	25	300	290	VLBA	16%
Fort Davis	FD	USA	25	300	290	VLBA	16%
Hancock	HN	USA	25	300	290	VLBA	16%
Kitt Peak	KP	USA	25	300	290	VLBA	16%
Los Alamos	LA	USA	25	300	290	VLBA	16%
Mauna Kea	MK	USA	25	300	290	VLBA	16%
North Liberty	NL	USA	25	300	290	VLBA	16%
Owens Valley	OV	USA	25	300	290	VLBA	16%
Pie Town	PT	USA	25	300	290	VLBA	16%
Saint Croix	SC	USA	25	300	290	VLBA	16%
Spacecraft							
VSOP	—	in orbit	8	17400	15300	—	—

1. The two letter codes used to represent individual telescopes with the exception of the codes VLBA and EVN that indicate the entire VLBA or EVN arrays that operate at a given frequency. These code letters must be used when specifying ground arrays of individual telescopes or the VLBA and EVN arrays in the VSOP proposal Cover Sheets.
2. The system equivalent flux density (SEFD), also known as the system temperature in Jy, is the ratio of the system temperature in K to the antenna sensitivity in K Jy^{-1}.
3. This column is the percentage of time that each telescope or array has committed to supporting the VSOP mission during AO phase 2 observations.
4. Cambridge is available for VLBI only during joint EVN/MERLIN sessions.
5. Use of the Green Bank 43 m (140′) telescope is not guaranteed after 1998.
6. The Cambridge, Lovell, and MK II telescopes all share both a VLBA and MkIV recorder. The default usage is for the MkIV recorder to be used by the Lovell or Mk II telescopes and the VLBA recorder is used with the Cambridge telescope.
7. It is expected that the Noto, Shanghai, Torun, and Cambridge VLBA recorders will be upgraded to MkIV recorders by 1999.
8. A VLBA recorder is expected to be available at Arecibo from Spring 1999 onwards.

8 VLBI Recorders and Correlators

8.1 VLBI Recorders

The tracking stations and ground radio telescopes used to support the VSOP mission will use four different recording systems to record the VLBI data. These recording systems are: VSOP-T, VLBA, MkIV and S2. Only one of the three VSOP observing modes, the mode with two 16 MHz two-bit sampled channels (see §3), can be supported by the VLBA, MkIV and S2 systems. All the tracking stations are equipped with both VLBA and S2 recorders. The Usuda tracking station is also equipped with a VSOP-T recorder. These recording systems use different physical media and it is a non-trivial exercise to cross-correlate data recorded on different recording systems with one another except for data recorded on VLBA and MkIV recorders.

8.2 Correlators and Tape Copiers

Table 7: Correlator Properties

Correlator	Location	Stations	Format	Min data dump time (seconds)	Max number of frequency channels /16 MHz/baseline
VLBA	Socorro, NM, USA	20	VLBA/MkIV	0.131	1024
VSOP	Mitaka, Japan	10	VSOP-T	0.025	4096
Canadian S2	Penticton, BC, Canada	6[1]	S2	0.001[2]	8192[3]
JIVE	Dwingeloo, Netherlands	16	MkIV/VLBA	1	1024[4]

Table 8: Tape Copiers at the VSOP Correlator

Copier			Number
VLBA	$\rightarrow$	VSOP-T	2
S2	$\leftrightarrow$	VSOP-T	2

1. Increase to 7-stations is planned. More than 6-stations can be processed with multiple automatic correlation passes.
2. See §9.12 for more details.
3. Very high spectral resolution is possible, using a digital zoom filter, see §9.11 for more details.
4. Actual number depends on exact experiment configuration. For example, 4096 frequency channels per 16 MHz per baseline are possible for an 8-station observation.

A comparison of the correlators that are able to support correlation of VSOP data is shown in Table 7. VLBI experiments using exclusively VLBA and MkIV recording systems are correlated on the VLBA correlator. All other experiments that use either S2 recorders or are mixed-mode, i.e., use more than one type of recorder (with the exception of VLBA and MKIV recorders) are correlated on either the VSOP or Canadian correlators. It should be noted that mixed-mode experiments (again with the those using VLBA and MKIV recorders) require tape-copying at Mitaka before they can be correlated. Table 8 shows that during the AO2 period there will be 2 uni-directional VLBA to VSOP-T tape copying machines and 2 bi-directional S2 to VSOP tape copying machines. There is also a plan not yet implemented to make the VLBA to VSOP-T copying machines bi-directional. Also shown in the table are the minimum correlator dump time in seconds and the maximum number of frequency channels per 16 MHz per baseline.

The Joint Institute for VLBI in Europe (JIVE) is building a 16 station MkIV correlator. This correlator may become operational for space VLBI observations in late 1999, and if this is the case will be used to correlate VSOP experiments involving the EVN. In general, NRAO has committed the VLBA correlator to processing experiments involving NRAO telescopes, including the VLBA and the VLA. Until the JIVE correlator becomes operational the VLBA correlator also correlates 20 hours per month of EVN-only VSOP observations.

There is no requirement for PIs to be present during correlation. The PI is sent the correlated VLBI data on either Exabyte or DAT tape and the necessary telescope calibration files are either attached to the correlated data or can be obtained by ftp from the the same ftp servers that are used for ground-based VLBI experiments. Additionally HALCA calibration files are placed on a ftp server at ISAS. For more details on how to obtain the calibration files consult the URL:

http://www.vsop.isas.ac.jp/obs/GRTcal.html

For AO2 experiments correlated with the VLBA correlator it is expected the calibration data will be included on the VLBI data distribution tape. The PI gets to choose the medium for their correlated data when they are sent an e-mail with the schedule of their observations 3–4 weeks before the observation. Experiments are typically correlated in less than 30 days after the experiment has taken place since there is a finite tape pool and tapes must be recycled in a timely fashion. After correlation has been judged complete and correct at a correlator, the tapes are erased and re-used. The PI has no option to ask that the raw tapes be kept until final data analysis is complete.

9 Observational Capabilities of the VSOP Mission

In this section the proposer is provided with the necessary information to calculate the resolution, the baseline sensitivity, the image sensitivity, and the field of view that one can obtain with VLBI observations using HALCA and co-observing ground radio telescopes. There is also a discussion of the polarization, spectral line, and pulsar observing capabilities of the VSOP mission. At various points in this section, examples will be illustrated by comparison to real space VLBI data obtained during the in-orbit-checkout phase of the VSOP mission. Figure 6 shows a comparison of the ground-only (VLBA) and ground-space (VLBA+VSOP) 1.6 GHz images resulting from real data, from observations of the source 1156+295 in June 1997. Figure 6 will be discussed further in the following subsections.

It should be noted that, although the increase in image resolution due to VSOP is obvious, the VLBA+VSOP image in Figure 6 is not an optimal observation but typical of the data obtained early in the in-orbit-checkout phase of the mission. For example, the experiment consists of only 2.5 hours of data, rather than the 7–14 hours that are now obtained during a General Observing Time observation. More examples of images made with HALCA can be found at the URL:

http://www.vsop.isas.ac.jp/general/Images.html.

9.1 Resolution

The resolution for an observation depends on the orientation of the source with respect to the orbit normal. For a source that lies along the direction of the orbit normal (or anti-normal), the full width half maximum (FWHM) beam size along the direction of the beam minor axis, θ_{minor}, is related to the observing frequency, ν, as follows:

$$\boxed{\theta_{\mathrm{minor}} \approx 1.2 \left(\frac{\nu}{GHz}\right)^{-1} \mathrm{mas}} \tag{7}$$

Similarly the FWHM beam size along the direction of the beam major axis, θ_{major}, is related to the observing frequency, ν, as follows:

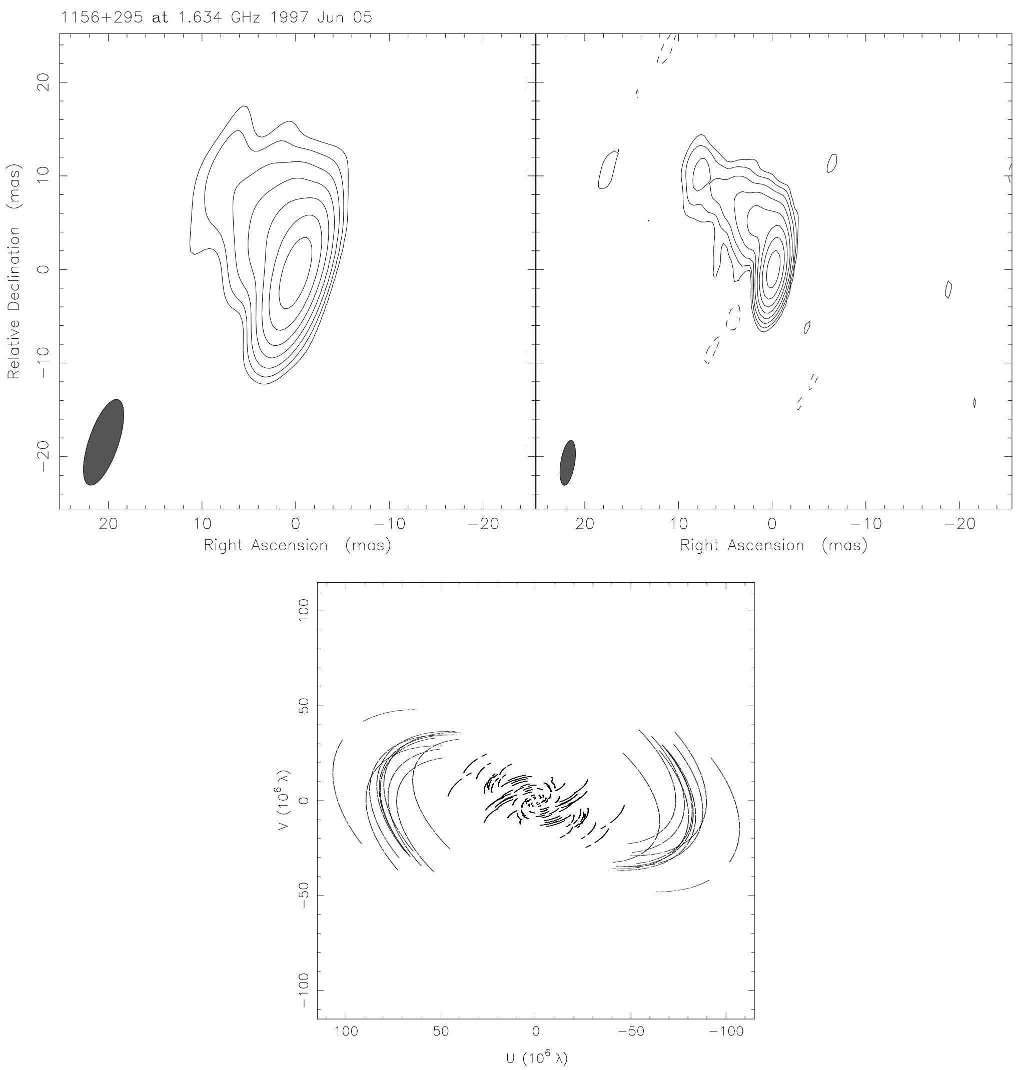

Figure 6: Top left: ground-only (VLBA) 1.6 GHz image of 1156+295 at 1.634 GHz from 1997, June 5. Contour levels are -1, 1, 2, 4, 8, 16, 32, and 64% of the peak, 1.13 Jy/beam. Beam FWHM, 9.6×3.2 mas at $-18.8°$. Top right: ground-space (VLBA+VSOP) 1.6 GHz image from same observation. Contour levels are -0.5, 0.5, 1, 2, 4, 8, 16, 32, and 64% of the peak, 0.99 Jy/beam. Beam FWHM, 4.9×1.5 mas at $-9.2°$. Bottom: the u-v coverage of the VLBA+VSOP observation.

$$\boxed{\theta_{\mathrm{major}} \approx 2.3\left(\frac{\nu}{GHz}\right)^{-1} \mathrm{mas}} \tag{8}$$

For sources that do not lie along the orbit normals, the FWHM major and minor beam sizes will be greater than or equal to the values quoted above. Furthermore the above beam sizes are those for an observation with HALCA and the VLBA using uniform weighting with each visibility weighted by the RMS noise level to the power $-\frac{1}{4}$. The beam size is a function primarily of the orientation of the source with respect to the orbit normal and the weighting scheme used. It depends only secondarily on the ground array used. It should also be noted that the FWHM minor axis beam size quoted above is 65% of the size of the fringe spacing for the longest baseline. This is quite consistent with the weighting scheme used.

Example: For a HALCA observation at 5 GHz, in the direction of the orbit normal, $\theta_{\mathrm{minor}} = 0.24$ mas and $\theta_{\mathrm{major}} = 0.46$ mas.

9.2 Baseline Sensitivity

The RMS thermal noise (σ_{ij}) in the visibility amplitude of a single polarization on a baseline between the i-th and j-th antennas in a VLBI array is given by:

$$\boxed{\sigma_{ij} = (\eta_s^{-1})\sqrt{\frac{T_i(Jy)T_j(Jy)}{2B\tau}}} \tag{9}$$

where:

η_s = The VLBI system efficiency factor (always < 1). This factor accounts for losses in the VLBI system (e.g. quantization in the data recording and correlator approximations). For 1-bit (2 level) sampling the VLBI efficiency factor is 0.64 while for 2-bit (4 level) sampling this factor is 0.88 (assuming that correlator losses are small).

$T_i(Jy)$ = The SEFD (system temperature in Jy) for the i-th antenna. See Table 6 for the value of this parameter.

$T_j(Jy)$ = The SEFD (system temperature in Jy) for the j-th antenna. See Table 6 for the value of this parameter.

B = The bandwidth in Hz. Theoretically for VSOP continuum observations the value of this parameter is either 32 or 64 MHz (see Table 2 for more details). In practice, it maybe more appropriate to use 16 MHz in fringe fitting SNR calculations for the VSOP observing mode that is compatible with all recording terminals since typically data from each 16 MHz baseband channel is independently fringe-fitted.

τ = The integration period in seconds. For fringe-fitting calculations, τ is the fringe-fitting interval. This should be about equal to the coherence time. See Table 9 for estimated values of the coherence time. For visibility data, τ is the integration period of each visibility point. This integration period can be, and often is, smaller than the coherence time.

Example: At 5 GHz, σ_{ij} is 21 mJy for HALCA to a single 25m VLBA antenna (assuming $T_{\mathrm{HALCA}} = 15300$ Jy, $T_{\mathrm{VLBA}} = 290$ Jy, B = 16 MHz, $\tau = 400$ s and $\eta_s = 0.88$).

Example: At 5 GHz, σ_{ij} is 6 mJy for HALCA to the 100m Effelsberg antenna (assuming $T_{\mathrm{HALCA}} = 15300$ Jy, $T_{\mathrm{Effelsberg}} = 20$ Jy, B = 16 MHz, $\tau = 400$ s and $\eta_s = 0.88$).

Table 9: HALCA (90%) Coherence Times (τ)

Observing Band	1.6 GHz	5 GHz
τ (seconds) ($>$ 1 hour from perigee)	$\sim$600	$\sim$400
τ (seconds) ($<$ 1 hour from perigee)	$\sim$400	$\sim$150

9.3 Fringe Fitting Signal to Noise Ratio

When fringe fitting VLBI data, the signal to noise ratio (SNR) on the baseline between the i-th and j-th telescopes in a VLBI array, SNR_{ij}, is given by:

$$\boxed{\mathrm{SNR}_{ij}(\tau) = \frac{C(\tau)S_c}{\sigma_{ij}(\tau)}} \qquad (10)$$

where $C(\tau)$ is the coherence function, S_c is the correlated flux density of the source and $\sigma_{ij}(\tau)$ is the RMS noise level, given by Equation 9. Over the fringe-fitting interval, τ, the amplitude of the correlated signal is degraded due to atmospheric irregularities and noise in the frequency standards or in the case of HALCA un-modelled accelerations. C(τ) measures this degradation. To obtain the highest signal to noise when fringe fitting, the fringe fitting interval needs to be chosen such that the SNR, given by Equation 10, is a maximum. A reasonable choice of τ is that for which C(τ) = 0.9. Table 9 shows the values of this interval as measured at the VLBA correlator. For more details about the coherence values in the Table 9 please consult the memo by Ulvestad, 1998 (http://www.nrao.edu/~julvesta/aoc/vtrep/halca_coher.ps). As can be seen the coherence time is reduced when HALCA is within a hour of perigee passage. Note that Equation 10 requires that the correlated flux density be used and not the total source flux density. Section 9.5 gives a method of how the correlated flux density can be predicted for Earth-space baselines.

Example: At 5 GHz, the SNR is 24 between HALCA and a single VLBA antenna for a 1 Jy circular Gaussian source with a brightness temperature of 1.22×10^{12} K observed on a projected baseline of 25,000 km (assuming T_{HALCA} =15300 Jy, T_{VLBA} = 290 Jy, B = 16 MHz, τ = 400 s, $C(\tau)$ = 0.9, and η_s = 0.88). See Equation 15 for how to calculate the correlated flux density.

Example: At 5 GHz, the SNR is 90 between HALCA and the 100m Effelsberg antenna for a 1 Jy circular Gaussian source with a brightness temperature of 1.22×10^{12} K observed on a projected baseline of 25,000 km (assuming T_{HALCA} =15300 Jy, $T_{\mathrm{Effelsberg}}$ = 20 Jy, B = 16 MHz, τ = 400 s, $C(\tau)$ = 0.9, and η_s = 0.88). See Equation 15 for how to calculate the correlated flux density.

9.4 Fringe Detection Limit

One important step in the processing of VLBI data after correlation is that the data must be fringe fit. In fringe fitting data, for ground-based VLBI, a search is made in delay and delay-rate space to find the fringe. For Space VLBI it may also be necessary to search in the delay-acceleration dimension as well, although the fringe fitting of in-orbit-checkout data obtained on the VSOP baselines has not required acceleration searches. If the search space is large then a high minimum SNR is required to guard against the probability of false fringe detection. For space VLBI the size of the search space is critically dependent on the size of the position, velocity and acceleration errors in the HALCA orbit. Experience obtained during AO1 observations has shown for a VLBI experiment with HALCA , a reasonable practical constraint on the minimum SNR useful for detecting fringes on the baselines to HALCA is:

$$\boxed{\mathrm{SNR_{min}} \sim 5 - 8} \tag{11}$$

However, it is strongly recommended that, during data reduction, the user attempt many fringe-fitting trials while varying $\mathrm{SNR_{min}}$, to determine an empirical value which is optimal for the array, source, and experimental setup particular to the observation in question. In certain circumstances using baseline stacking in fringe-fitting it is possible with due care and diligence to increase the signal from HALCA. The minimum SNR can be reduced by using narrower delay and rate search search windows. However, it is recommended that proposers use the above limit when trying to estimate the fringe detection limit on baselines to HALCA. Proposers need to convince themselves and the Scientific Review Committee that there is reasonable chance that SNR_{ij} will exceed $\mathrm{SNR_{min}}$ on baselines to HALCA having projected lengths of order 25,000 km.

9.5 Estimated Correlated Flux Density

The SNR formula (Equation 10) requires that the correlated flux density, S_c, be used. Except for a point source, the correlated flux density is always less than the total flux density of the source. Thus, in order to predict if fringes will be detected on baselines to HALCA, we need a method of predicting the correlated flux density on these baselines. In the two methods described below, we treat the source as a single Gaussian component. In reality it is known that VLBI sources in general have complex morphology. Therefore the methods described below should be applied to the most compact VLBI component in a VLBI source, which for most extragalactic sources is the radio core.

9.5.1 Using the Source Size

If we assume that the source has a circular Gaussian brightness distribution, then the correlated flux density, S_c, measured on a projected baseline of length D is related to the total source flux density, S_0, and the full width half maximum size of the source, θ_{FWHM}, as follows:

$$\boxed{S_c = S_0 e^{-0.093(\frac{D}{10^4\,km})^2(\frac{\theta_{FWHM}}{1\,mas})^2(\frac{\nu}{1\,GHz})^2}} \tag{12}$$

Example: At 5 GHz, the correlated flux density is 0.56 Jy for a 1 Jy circular Gaussian source with $\theta_{FWHM} = 0.2$ mas observed on a projected baseline length of 25,000 km.

9.5.2 Using the Source Brightness Temperature

A useful way to characterize the monochromatic surface brightness of a radio source is to determine the physical temperature that a black body radiator would need to possess to produce the same observed surface brightness. This temperature is known as the brightness temperature of the radio source. For a circular Gaussian source the maximum brightness temperature, T_b, is related to the component flux density, S_0, the component full width half maximum size, θ_{FWHM}, and the observing frequency, ν, as follows:

$$\boxed{T_b = 1.224 \times 10^{12}(\frac{S_0}{1\,Jy})(\frac{\theta_{FWHM}}{1\,mas})^{-2}(\frac{\nu}{1\,GHz})^{-2}\,\mathrm{K}} \tag{13}$$

Example: At 5 GHz, the brightness temperature is 1.22×10^{12} K for a 1 Jy circular Gaussian source with $\theta_{FWHM} = 0.2$ mas.

Alternatively if the source brightness temperature is known and the source is again assumed to be a circular Gaussian, Equation 13 may be inverted to solve for the component full width half maximum size, θ_{FWHM}, in terms of the maximum brightness temperature, T_b, the component flux density, S_0, and the observing frequency, ν, as follows:

$$\boxed{\theta_{FWHM} = 1.106\,(\frac{S_0}{1\,Jy})^{\frac{1}{2}}(\frac{T_b}{10^{12}\,K})^{-\frac{1}{2}}(\frac{\nu}{1\,GHz})^{-1}\ \mathrm{mas}} \qquad (14)$$

Assuming a circular Gaussian source brightness distribution, the correlated flux density, S_c, is related to the brightness temperature, T_b, projected baseline length, D, and the observing frequency, ν, as follows:

$$\boxed{S_c = S_0\, e^{-0.114(\frac{S_0}{1\,Jy})(\frac{D}{10^4\,km})^2(\frac{T_b}{10^{12}\,\mathrm{K}})^{-1}}} \qquad (15)$$

Example: At 5 GHz, the correlated flux density is 0.56 Jy for a 1 Jy circular Gaussian source with a brightness temperature 1.22×10^{12} K observed on a projected baseline of 25,000 km.

The equations presented above (12 and 15) should not be taken as the definitive answer of what the correlated flux density will be on baseline lengths exceeding an Earth diameter. These equations are if anything a conservative approximation. Results from the TDRSS space VLBI experiments (Linfield *et al*, 1989 and Linfield *et al*, 1990) and ground-based VLBI have shown that a common property of radio sources is that they often have more correlated flux density on long baselines than is obtained by extrapolating simple Gaussian models derived from short baseline data.

9.6 Field of View

The field of view of a space VLBI observation, practically speaking, is limited by two effects which are examined in the following subsections. A third limitation, an effect of non-coplanar phase residuals, will typically be measured in arcseconds for space VLBI observations and is, therefore, insignificant.

9.6.1 Bandwidth Smearing

Due to the finite observing bandwidth, the visibility amplitude of a point source not located at the phase center is degraded. In order that this degradation is limited to only P%, the limit on the field of view, θ_B, that is a function of both the observing bandwidth, B, and the baseline length, D, is as follows:

$$\boxed{\theta_B = 60\,P^{\frac{1}{2}}(\frac{B}{16\,MHz})^{-1}(\frac{D}{10^4\,km})^{-1}\ \mathrm{mas}} \qquad (16)$$

Example: If the visibility amplitude is to be degraded by less than 5%, the field of view is limited to less than 54 mas by this effect for an observation with a bandwidth of 16 MHz on a baseline of 25,000 km.

Comparison to 1156+295: For the in-orbit-checkout observation of 1156+295, $B = 16$ MHz (only half the available bandwidth was used), $D = 1.3 \times 10^4$ km, and $\theta_B = 15$ mas (maximum extent of source structure). Thus, the degradation of the visibility amplitude over the field of view is 0.1%.

9.6.2 Time Average Smearing

Due to the finite integration time of each visibility point, the visibility amplitude of a point source not located at the phase center is degraded. Fundamentally, it is the correlator dump time ($\sim$ 1 second) that limits the field of view due time-average smearing. However, it is fairly common practice to time average the visibility data before imaging the data. It is this time averaging of the data that may place a stricter limit on the field of view than bandwidth smearing depending on what visibility averaging time is used.

The general analysis of time average smearing for ground VLBI is difficult and is often restricted for simplicity to a source located at the north (or south) pole. For space VLBI there is an analogy to the ground north pole case, and that is to consider a source located along the orbit normal. Due to the different spacecraft velocities at apogee and perigee, the fields of view are different at these two locations and we will consider both cases. The spacecraft velocity at apogee, v_a, and at perigee, v_p, depend on the spacecraft orbital period, T, orbit eccentricity, e, and orbit semi-major axis, a, as follows:

$$\boxed{\mathrm{v}_a = \frac{2\pi a}{T}\sqrt{\frac{(1-e)}{(1+e)}} \text{ and } \mathrm{v}_p = \frac{2\pi a}{T}\sqrt{\frac{(1+e)}{(1-e)}}} \quad (17)$$

Example: v_a and v_p are 2.4 $\mathrm{km\,s^{-1}}$ and 9.6 $\mathrm{km\,s^{-1}}$ respectively for the nominal VSOP spacecraft orbit listed in Table 4.

In order that the visibility amplitude degradation due to time average smearing is limited to only P%, the limit on the field of view at either apogee or perigee, θ_τ, is a function of the observing frequency, ν, the visibility averaging time, τ_v, and the spacecraft velocity, v, is as follows:

$$\boxed{\theta_\tau = 96\, P^{\frac{1}{2}} (\frac{\nu}{1\, GHz})^{-1} (\frac{\mathrm{v}}{1\, kms^{-1}})^{-1} (\frac{\tau_v}{100\, sec})^{-1} \text{ mas}} \quad (18)$$

Thus, the field of view can be increased by reducing the visibility averaging time.

Example: If the degradation to the visibility amplitude is to be less than 5%, the field of view is limited to be less than 4.7 mas at apogee for a visibility averaging time of 400 seconds at 5 GHz. The corresponding limit on the field of view at perigee is 1.3 mas.

Comparison to 1156+295: For the in-orbit-checkout observation of 1156+295, τ_v = 30 sec, ν = 1.634 GHz, and θ_B = 15 mas. From Table 4 v_a and v_p are 2.4 $\mathrm{km\,s^{-1}}$ and 9.6 $\mathrm{km\,s^{-1}}$ respectively. Thus, at apogee the visibility amplitudes are degraded by 0.03% and at perigee by 0.51%.

Thus, there is a stricter limit on the field of view for data taken near perigee compared to apogee. Simply stated the field of view due to time average smearing is roughly 10 times smaller for observations with HALCA than with ground-based VLBI due to the high velocity of HALCA at perigee.

9.7 Imaging Sensitivity

Proposers wishing to make images need to work out if the expected RMS noise level on their images is low enough for them to meet the scientific goals of their experiment.

The RMS noise per beam on an image (for natural weighting), ΔI, is given by:

$$\boxed{\Delta I = \frac{\sqrt{\sum w_{ij}^2 \sigma_{ij}^2}}{\sum w_{ij}}} \quad (19)$$

where the summation is over all the visibilities in the experiment and w_{ij} is the weight attached to each visibility point and σ_{ij} is the RMS noise level on the visibility amplitude given by Equation 9. For a VLBI array of equal elements, it is easy to show that:

$$\boxed{\Delta I = \frac{\sigma_{ij}}{\sqrt{N}}} \tag{20}$$

where N is the number of visibility points and σ_{ij} is again the RMS noise level on the visibility amplitude. For an observation of a circumpolar source with an array of equal elements the above equation can be re-expressed in terms of the SEFD of an individual array element, T_i, the length of the observation, τ_{obs}, the bandwidth, B, the number of telescopes in the array, n_t, and the VLBI system efficiency factor, η_s, as follows:

$$\boxed{\Delta I = \eta_s^{-1}\frac{T_i}{\sqrt{n_t(n_t-1)B\tau_{obs}}}} \tag{21}$$

Example: At 5 GHz, for a VLBA-only (n_t=10) experiment on a circumpolar source that lasts 18 hours, ΔI= 25 μJy per beam (assuming $T_{\rm VLBA}$ = 290 Jy, B = 32 MHz and η_s = 0.88).

The extension of Equation 21 to an array of non-equal elements, like the EVN or the addition of HALCA to the VLBA say, is as follows. For such an array we can define a single SEFD number, $< T_i >$, such that the above equation is true for the array, if we substitute $< T_i >$ for T_i. It can be shown that $< T_i >$ is given by:

$$\boxed{< T_i >= \sqrt{n_t(n_t-1)}\frac{\sqrt{\sum_i \sum_{j\neq i}(T_iT_j)^{1-m}}}{\sum_i \sum_{j\neq i}(T_iT_j)^{-\frac{m}{2}}}} \tag{22}$$

In deriving the above expression the weight attached to each visibility point is chosen to be inversely proportional to the RMS noise raised to some power m ($w_{ij} = \sigma_{ij}^{-m}$). For optimum weak source detection $m = 2$. However many VLBI astronomers choose $m = \frac{1}{4}$ for VLBI arrays that contain antennas with a wide range of SEFD values. There is a trade-off to be made for space VLBI as to what is the best value to choose for m. With a lower value of m higher resolution images will be obtained but the beam side-lobe level and the image noise level will be higher. For Figure 6, $m = 1$ was adopted, after many imaging trials, as a good compromise. Also, Figure 6 was produced using uniform weighting, rather than natural weighting, to emphasize the visibilities on the long space baselines, over the higher SNR short baseline visibilities.

Example: For the EVN antennas listed in Table 6 using Equation 22, it can be shown that for m = 1/4, $< T_i >$ is 270 Jy (n_t=9) and 230 Jy (n_t=9) at 1.6 GHz, and 5 GHz respectively. As the number of elements in the EVN array and the $< T_i >$ values are similar to the values for the VLBA the noise level obtained with a ground observation only with the EVN is similar to what is obtained with the VLBA. The error made by using a simple average for the EVN, $(1/n_t)\sum_i T_i$ as an approximation to $< T_i >$, is to overestimate this value by $\approx$ 38% and $\approx$ 18% at 1.6 GHz, and 5 GHz respectively (for m = 1/4).

There is a useful extension to Equation 22 and that is to consider the addition of HALCA to a ground array. In that case, the RMS noise level on the image, ΔI_{space}, is related to the RMS noise level obtained with the ground array alone, ΔI_{ground}, as follows:

$$\Delta I_{space} = \Delta I_{ground} \frac{\sqrt{1+\frac{2}{n_g-1}\left(\frac{T_v}{<T_g>}\right)^{1-m}}}{\left(1+\frac{2}{n_g-1}\left(\frac{T_v}{<T_g>}\right)^{-\frac{m}{2}}\right)} \qquad (23)$$

where n_g is the number of the antennas in the ground array and $\frac{T_v}{<T_g>}$ is the ratio of HALCA SEFD to the ground array SEFD, calculated using Equation 22. In the above expression the weight attached to each visibility point is chosen to be inversely proportional to the RMS noise raised to some power m ($w_{ij} = \sigma_{ij}^{-m}$).

Example: At 5 GHz for a VLBA experiment with HALCA of a circumpolar source that lasts 18 hours, assuming that the source is always visible for HALCA, $\Delta I_{space} = 25$ μJy per beam for $m = 2$ and 50 μJy per beam for $m = \frac{1}{4}$ (assuming $T_{\rm VLBA} = 290$ Jy, $T_{\rm HALCA} = 15300$ Jy, $B = 32$ MHz, and $\eta_s = 0.88$).

Comparison to 1156+295: For the 1156+295 observations discussed at the start of this section ($\nu =$ 1.6 GHz, $B = 16$ MHz, T_{VLBA} =300 Jy, T_{HALCA} =17400 Jy, $\eta_s = 0.88$, $n_g = n_t = 10$, and $\tau_{obs} = 2$ hours), it is possible to calculate the expected image sensitivity for naturally weighted images, using different values of m, from Equations 21 and 23. For $m = 0$, $\Delta I_{space} = 0.3$ mJy/beam. For $m = 1$, $\Delta I_{space} = 0.1$ mJy/beam. For $m = 2$, $\Delta I_{space} = 0.1$ mJy/beam. From Table 10, one can see that the image sensitivities actually achieved from 1156+295, for $m = 0, 1, 2$, are approximately 10 – 20 times higher than predicted. This is probably due to the presence of amplitude calibration errors in the data of between 5 and 10%, as discussed in the following section on dynamic range.

Table 10: Results of 1156+295 imaging trials, natural weighting

m	Peak Jy/beam	RMS mJy/beam	Dyn. range	Beam$_{maj}$ mas	Beam$_{min}$ mas	Beam P.A. °
0	0.96	1.9	500:1	6.7	2.1	−5.9
1	1.03	1.4	740:1	9.4	3.5	−9.8
2	1.06	1.1	960:1	10.6	4.6	−13.1

For completeness, Table 11 lists the results for imaging trials of 1156+295 using uniform weighting schemes and $m = 0, 1, 2$. As mentioned above, Figure 6 was produced using uniform weighting and $m = 1$.

Table 11: Results of 1156+295 imaging trials, uniform weighting

m	Peak Jy/beam	RMS mJy/beam	Dyn. range	Beam$_{maj}$ mas	Beam$_{min}$ mas	Beam P.A. °
0	0.94	7.9	120:1	3.7	1.1	−7.3
1	0.99	1.5	660:1	4.9	1.5	−9.2
2	1.01	1.3	780:1	7.2	2.3	−12.8

9.8 Dynamic Range

The dynamic range of an image is defined as $P_+/\Delta I_m$, where P_+ is the peak flux density in the image in units of Jy/beam and ΔI_m is the measured RMS noise level on the image also in units of Jy/beam. It should be noted that the definition of dynamic range uses the measured image RMS noise level (ΔI_m) and not the theoretical number (ΔI) calculated using Equation 19. In VLBI images ΔI_m can be significantly higher than ΔI. For example, if the measured noise on the image was equal to the predicted thermal noise then the dynamic range in the previous example for a 1 Jy point source would be $\approx$ 20,000:1. One of the main reasons for this is that the RMS noise level on a visibility point can exceed the thermal noise level predicted by Equation 9 due to systematic amplitude calibration errors. In VLBI amplitudes are typically calibrated to a few percent. Consider the case of an observation of a 1 Jy point source with each visibility point having 5% amplitude errors (1 σ) distributed as a Gaussian about the true 1 Jy value. In this case σ_{ij} would be 50 mJy. For an observation with HALCA and a 10 element ground array for 18 hours the number of visibility points is $\approx 10^4$, assuming a visibility integration period of 350 seconds. Hence according to Equation 20 the RMS noise level on the map is expected to be $\approx$ 0.5 mJy and the dynamic range is this case would be $\approx$ 2000:1. Calibrating the HALCA antenna is different from what is normally encountered in ground-based VLBI (see §12 for details) and proposers should therefore proceed with caution when estimating the dynamic range that will be achieved. In addition to amplitude calibration errors, the low sensitivity of HALCA baselines and the sometimes poor (u,v) coverage of space VLBI observations may also reduce the achievable imaging dynamic range of space VLBI data. The actual dynamic range achievable may be a factor of 10 worse than predicted by using thermal noise calculations such as Equation 19.

To date, the highest dynamic range of a HALCA image is ~1000:1.

9.9 Typical VSOP Observations

Typical observations in General Observing Time have last 7–14 hours. Every effort is made to schedule an observation with the best (u,v) coverage that can be obtained on the source given the constraints. For more details on the VSOP scheduling process see §11.

9.10 Polarimetry

When performing VLBI polarization observations, one usually thinks in terms of a VLBI experiment in which all telescopes record simultaneously both the left- and right-circularly-polarized (LCP and RCP) signals incident from a compact radio source. Information about the distribution of the total intensity emission and possibly the circularly polarized emission is derived from the sum (Stokes I) or difference (Stokes V) of the $L \otimes L$ and $R \otimes R$ ("parallel-hand") correlations. Information about the distribution and position angle of linearly polarized emission is derived from the sum (Stokes Q) and difference (Stokes U) of the $R \otimes L$ and $L \otimes R$ ("cross-hand") correlations. With modern ground-based arrays (e.g., the VLBA) that were designed with polarization observations in mind, such experiments are becoming more routine. However, for several reasons, polarization observations with HALCA will be considerably more difficult than the ground-based case.

First, HALCA receives only one hand of circular polarization (LCP). Unlike the *real* total intensity image, the *complex* linear polarization image requires both cross-hand correlations for each baseline to symmetrically sample the (u,v) plane. Since only one of the two cross-hands will be available from HALCA correlations (ground telescopes will observe both LCP and RCP), only half of the (u,v) plane will be filled with polarized visibilities on the space baselines. While formation of polarization images is still possible via complex deconvolution techniques developed to accommodate this difficulty in ground-based VLBI polarimetry, proposers should be aware that full-resolution space VLBI polarization imaging (like total intensity space VLBI imaging) will have stricter dynamic range limitations than is typically realized in full-polarization ground-based VLBI.

The second, and more fundamental issue connected with space VLBI polarization observations is calibration of HALCA's instrumental contribution to the polarization visibilities, i.e., it's feed impurity.

Like circularly polarized feeds on ground radio telescopes, HALCA's LCP feed's response to RCP is not identically zero. Since this 'leakage' of RCP will correlate with the RCP signal from ground radio telescopes at a level proportional to the total intensity correlation of the radio source, it must be calibrated and removed. For ground arrays, this calibration has traditionally been achieved by making observations of a source of known (usually zero) polarization as it diurnally rotates in the field of view of the telescopes. Since the instrumental contributions (assumed constant) of each telescope rotate differentially in phase with respect to those of the others as well as to the source contribution, the instrumental contribution of each feed may be solved for. More recently, it has become possible to solve for both the instrumental *and* the source polarization (with some assumptions about the polarized intensity distribution), thus eliminating the need for a calibrator of known polarization.

Unlike ground telescopes used for VLBI polarimetry, HALCA cannot slew to sources of known polarization and it does not rotate about the source direction. Therefore, it will be difficult to calibrate HALCA's feed impurity by conventional means. Additional difficulties may arise if the polarization impurity is significantly variable in a non-predictable way on the timescale of the observations. Such variations could be caused, for example, by changes in the shape of the HALCA antenna as it comes out of eclipse. Furthermore, the polarization properties of the antenna may also be a function of the angle between the source and the Sun.

Possibilities for achieving reliable polarization calibration for HALCA are currently under investigation by a Polarization Study Team established by the mission. It is expected that the ground array instrumental polarization will be calibrated independently, then simultaneous solutions for HALCA's polarization impurity and the source structure *on space VLBI scales* will be obtained and tested for consistency with the ground-only results. As polarization calibration results become available in March and April, the Polarization Study Team will report them on the VSOP WWW site (http://www.vsop.isas.ac.jp).

In addition to the fundamental issues described above, there are several logistical issues to be considered when planning space VLBI polarimetry with HALCA.

First, since HALCA polarization observations will require recording of both RCP and LCP at all capable ground telescopes, the default observing mode at these telescopes will be to record one, 2-bit sampled, 16 MHz IF channel each in both RCP and LCP (please refer to §3 and Table 2 for a description of the available HALCA recording modes) and one of the HALCA IF channels will be discarded. This is necessary to avoid doubling the tape requirements at these stations by increasing the total bit-rate from 128 Mbit/s to 256 Mbit/s. However, the larger bit rate will be considered, and the full HALCA bandwidth used, if a sufficiently strong scientific case is made. Another option–a mode in which the ground telescopes record both 16 MHz IF channels with *1-bit* sampling in both polarizations–yields better sensitivity than the single channel mode while maintaining the 128 Mbit/s bit-rate limit at the ground telescopes. Unfortunately, this mode is currently not available due to limitations in the current FITS specification for correlator output data. Should this change, and this mixed mode become available, it will likely become the default for polarization observations.

Second, it is usually necessary to obtain a calibration of the electric vector position angle for polarization observations. In practice, this reduces to calibrating the phase difference between the RCP and LCP systems at the reference antenna and is usually achieved by including observations of a highly-polarized compact source (e.g., a BL Lacertae object) for which the correct position angle of the integrated emission is known or measurable with time granted by an independent single-dish telescope or the VLA. Since this property of the reference antenna can be measured with ground telescopes alone, the observational constraints of HALCA have no direct bearing on obtaining this calibration. In fact, in typical HALCA imaging observations, there are usually several gaps in the tracking station coverage during which the ground array could observe such calibrators. However, since scheduling of the ground array will be undertaken by the VSOG, proposers should explicitly indicate their requirements in this regard on their cover sheets (with supporting text in their justification), including a list of acceptable calibrators. Proposers should assume responsibility for separately obtaining the supporting single-dish observation, although it is possible that appropriate ground telescopes may be scheduled as part of the HALCA observation which would be similarly available during the HALCA tracking gaps, and thus could be properly scheduled for this purpose. Also, if the 256 Mbit/s recording rate is desired, proposers should be aware that very little tape may be available for periods when HALCA is not observing, i.e., observations of the proposed target source are given priority by default to maximize the space-baseline coverage of all observations.

9.11 Spectral Line Observations

The type of spectral line VLBI observations that may be conducted with the VSOP mission depend firstly on the properties of the VSOP spacecraft science subsystem, described in §3, and secondly on the properties of the correlator used to correlate the data. In this section we will assume the VSOP spacecraft is operating in the VLBA/MkIV/S2 compatible mode. In this mode the VSOP spacecraft has two 16-MHz channels and it is possible to independently set the frequency range of each of the two channels, provided that the lowest frequency in each channel is an integral number of MHz.

Table 7 compares the properties of the correlators that correlate VSOP observations including the maximum number of frequency channels per 16-MHz per baseline and the minimum correlator dump time or integration period.

For the VLBA correlator, each baseband channel can be resolved into as many as 1024 spectral points, subject to a maximum of 2048 points per baseline, independent of channel bandwidth. For HALCA's fixed 16-MHz channels, the highest velocity resolution will thus be only 3 km/s for OH masers. The output integration time can be any integral multiple of the 131.072-millisecond short-term integration cycle, subject to an overall output data rate limit of 0.5 Mbytes per second.

For the VSOP correlator 8192 spectral line channels per baseline are created and a maximum of 1024 spectral line channels can be output. These output channels can either be individual channels or combinations of channels from the 8192 channel data. Consequently the VSOP correlator can provide a factor of four higher spectral resolution compared to the VLBA correlator. Thus, the velocity resolution with the VSOP correlator for OH masers will be 0.73 $\mathrm{km\,s^{-1}}$. The minimum integration period of the VSOP correlator is 25 milliseconds and the maximum data output rate is 1.5 $\mathrm{Mbyte\,s^{-1}}$.

In a single pass the Canadian correlator can process all baselines with 256 or 512 frequency points per baseline, 12 baselines with 1024 frequency points, 6 baselines with 2048 frequency points, 3 baselines with 4096 frequency points, or 1 baseline with 8192 frequency points. Additionally, the correlator has a decimating digital filter that is used to implement a frequency 'zoom' mode whereby increased spectral resolution can be obtained on a narrower bandwidth. Zoom factors of 4x, 8x, 16x, and 32x can be achieved with a corresponding reduction in available bandwidth. E.g. for a zoom factor of 32, and 2048 frequency points, the usable bandwidth (assuming an input VSOP bandwidth of 16 MHz) is 500 kHz and the spectral resolution is 244 Hz. The penalty for using zoom mode is a reduction in SNR of 12% due to re-quantization after filtering. More baselines can be processed with high spectral resolution using multiple automatic correlator passes.

To recap the above discussion. If the desired frequency channel bandwidth is greater than or equal to 16 kHz then the VLBA correlator can be used. On the other hand, if narrower frequency channels are desired then the data must be correlated at either Mitaka or Penticton which in turn means that few ground telescopes with either VLBA or MKIV recorders may be used in the experiment due to the limited tape copying facilities.

As with continuum observations, spectral line observers need to convince the Science Review Committee that there is a reasonably good chance of detecting fringes on the baselines to HALCA. In practice this means that the spectral line source has been observed with ground-based VLBI and the correlated flux density on long Earth baselines in known.

9.12 Pulsar Observations

Observations of pulsars with HALCA are possible and this type of observation has already been made during the first AO. Gating will be needed in order to improve the signal to noise of the observations which will be available on Canadian S2 correlator and probably the VLBA correlator. Pulsar gating is not yet implemented on the VLBA correlator but it is expected that this will be available in the time-frame covered by the second AO period. Experiments which use the VLBA and other VLBA-format telescopes will be correlated in Socorro. Other experiments using the S2 or VSOP data recording format will be sent to Penticton. For some pulsars between -20 and -50 declination the use of S2 recording telescopes with a few VLBA telescopes would give good u-v coverage, but the double copying need from S2 to VLBA is not yet available.

The Canadian S2 correlator has a minimum correlator dump interval of 1.0 milliseconds and at this rate only 6 baselines can be processed at 128 lags (64 frequency points) per baseline. However, this fast dump mode is particularly useful for pulsar observations where it is combined with pulsar gating to keep the total data rate reasonable (e.g. with a gate on time of 10 msec and a period of 100 msec, and a dump time of 1.0 msec, then 100 dumps are generated per second). In fact, this fast dump mode is being used in the V029a Vela pulsar experiment to provide the PI with more information than would be obtained with simple gating. As the dump time increases (2 to 10msec), the spectral resolution increases as well but still only 6 baselines are available. If the dump time is >= 10 msecs, then more baselines and more spectral resolution are available.

It is important in the correlation of the VSOP data that the correct phasing of the gating is known. If the dispersion of the pulsar is large, the gating time frame versus frequency is also important. Both the Socorro and Penticton correlators do include dispersion in the gating information. The method for obtaining this gating information will depend on the strength of the pulsar and its regularity. For strong pulsars, it may be possible to determine the gating directly from the observations (for example the total power in some of the larger telescopes). For weaker pulsars, special observations (perhaps with other telescopes not involved with the VSOP experiment) may have to be made. Depending on the regularity of the pulsar, these additional observations may have to be made during or within a few days of the HALCA experiment. For some very regular pulsars, no additional observations may be needed.

About one month before the observations, please contact the VSOG about your experiment (vsog@vsop.isas.ac.jp) You should also contact the correlator to be used with your observations in order to determine the method in which the gating information is needed. For the Penticton correlator, please contact Brent Carlson (bcarlson@drao.nrc.ca); for the VLBA correlator, please contact Jon Romney (jromney@aoc.nrao.edu).

The processing and imaging of pulsar data, after correlations, should not differ from continuum observations.

10 Source Selection

It is up to the proposer to decide what to observe. However, to help the proposer in deciding what type of sources are observable with the VSOP mission both the sources of observed in the first AO period by the VSOP mission and the results from a ground-based 5 GHz survey are presented in this section.

10.1 Sources Observed During First AO Period

Table 12 provides a list of all sources that have been or are expected to be observed during the first AO period. The 'Other Names' column contains the more common names for the sources and typically includes the B1950 name.

For more up to date details on what sources have been observed during the first AO period please consult the URL:

http://www.vsop.isas.ac.jp/obs/ExpStatus.html

For observations that have not yet taken place please consult the URL:

http://www.vsop.isas.ac.jp/obs/longterm.html

Table 12: Sources Observed or Expected to be Observed During First AO Period

Source name	Band	Epochs	Other names	Source name	Band	Epochs	Other names
J0017+8135	L	1	0014+813	J1150+2417	C	1	1127+245
J0017+8135	C	1	0014+813	J1229+0203	L	1	1226+023 3C273 3C273B
J0019+7327	C	1	0016+731	J1229+0203	C	1	1226+023 3C273 3C273B
J0057+3021	L	1	0055+300 NGC315	J1230+1223	L	1	1228+126 VirA M87
J0057+3021	C	1	0055+300 NGC315	J1230+1223	C	1	1228+126 VirA M87
J0111+3906	C	1	0108+388	J1256-0547	L	1	1253-055 3C279
J0133+6226	L	1	OH127.8-0.0	J1256-0547	C	1	1253-055 3C279
J0136+4751	C	1	0133+476	J1310+3220	C	1	1308+326
J0157+7442	C	1	0153+744	J1325-4301	C	4	1322-427 CenA
J0203+1134	L	1	0201+113	J1335+4542	C	1	1333+459
J0203+1134	C	1	0201+113	J1343+6602	C	1	1342+662
J0210-5101	C	1	0208-512	J1354-0206	L	1	1351-018
J0217+7349	C	2	0212+735	J1354-0206	C	1	1351-018
J0222-1615	L	1	0219-164	J1357-1744	L	1	1354-174
J0226+3421	L	1	0223+341	J1357-1744	C	1	1354-174
J0226+3421	C	1	0223+341	J1405+0415	L	1	1402+044
J0227+6152	L	2	W3OH	J1405+0415	C	1	1402+044
J0237+2848	C	2	0234+285	J1407+2827	C	1	1404+286
J0238+1636	L	2	0235+164	J1415+1320	C	1	1413+135
J0240-2309	L	1	0237-233	J1445+0958	L	1	1442+101
J0251+4315	C	1	0248+430	J1445+0958	C	1	1442+101
J0319+4130	L	2	0316+413 3C84	J1459+7140	L	1	1458+718 3C309.1
J0319+4130	C	4	0316+413 3C84	J1459+7140	C	1	1458+718 3C309.1
J0332+5434	L	2	PSR0329+54	J1459-1641	L	1	1456-165 NGC5793
J0339-0146	L	1	0336-019 CTA26	J1522-2730	L	1	1519-273
J0406-3826	L	2	0405-385	J1522-2730	C	1	1519-273
J0414+0534	L	1	MG0414+0534	J1534+2330	L	1	ARP220
J0418+3801	L	1	0415+379 3C111	J1551+5806	C	1	1550+582
J0418+3801	C	1	0415+379 3C111	J1609+2641	L	1	1607+268 CTD93
J0423-0120	L	1	0420-014	J1616+0459	C	1	1614+051
J0423-0120	C	1	0420-014	J1623+6624	C	1	1622+663
J0433+0521	L	1	0430+052 3C120	J1625+4134	C	1	1624+416
J0433+0521	C	2	0430+052 3C120	J1632+8232	C	1	1637+826 NGC6251
J0440-4333	C	1	0438-436	J1635+3808	C	2	1633+382
J0508+8432	C	1	0454+844	J1638+5720	C	1	1637+574
J0519-4546	C	1	0518-458 PicA	J1642+3948	L	2	1641+399 3C345
J0522-3627	C	1	0521-365	J1642+3948	C	3	1641+399 3C345
J0530+1331	L	1	0528+134	J1642+6856	C	1	1642+690
J0530+1331	C	2	0528+134	J1644-4559	L	1	PSR1641-45
J0538-4405	C	1	0537-441	J1653+3945	L	1	1652+398 Mkn501
J0539-2839	L	1	0537-286	J1653+3945	C	1	1652+398 Mkn501
J0539-2839	C	1	0537-286	J1733-1304	L	1	1730-130 NRAO530
J0555+3948	C	1	0552+398 DA193	J1733-1304	C	1	1730-130 NRAO530
J0607+0005	L	1	MonR2	J1740+5211	C	1	1739+522
J0624+3856	L	1	0620+389	J1748+7005	C	1	1749+701
J0624+3856	C	1	0620+389	J1751+0939	C	1	1749+096
J0626+8202	C	1	0615+820	J1800+7828	L	1	1803+784
J0635-7516	C	1	0637-752	J1800+7828	C	3	1803+784
J0642+6758	C	1	0636+680	J1806+6949	C	2	1807+698 3C371
J0646+4451	L	1	0642+449	J1810+5649	C	1	1809+568
J0646+4451	C	1	0642+449	J1814+0018	L	1	W33A
J0650+6001	C	1	0646+600	J1824+5651	C	1	1823+568
J0714+3534	C	1	0711+356	J1829+4844	L	2	1828+487 3C380
J0721+7120	C	3	0716+714	J1829+4844	C	1	1828+487 3C380
J0728+6748	C	1	0723+679 3C179	J1842+7946	C	1	1845+797 3C390.3
J0738+1742	C	1	0735+178	J1853+0114	L	2	OH34.28+0.15
J0741+3112	C	1	0738+313	J1901+0113	L	1	W48
J0747+7639	C	1	0740+768	J1902+3159	C	1	1901+319 3C395
J0808+4950	C	3	0804+499	J1914+1109	L	1	OH45.5+0.1
J0818+4222	C	1	0814+425	J1924-2914	L	1	1921-293
J0825+6157	C	1	0821+621	J1924-2914	C	2	1921-293
J0831+0429	C	1	0829+046	J1927+7358	L	1	1928+738
J0835-4510	L	1	VELAPSR PSR0833-45	J1927+7358	C	5	1928+738
J0840+1312	C	1	0838+133 3C207	J1932+1059	L	1	PSR1929+10
J0841+7053	L	2	0836+710	J1939-1002	L	1	1937-101
J0841+7053	C	1	0836+710	J1939-1002	C	1	1937-101
J0854+2006	L	2	0851+202 OJ287	J1939-6342	C	1	1934-638
J0854+2006	C	2	0851+202 OJ287	J1940-6907	C	1	1935-692
J0903+4651	C	1	0859+470	J1955+5131	C	1	1954+513
J0909+4253	L	1	0906+430 3C216	J1959+4044	C	1	1957+40 CygA
J0909+4253	C	1	0906+430 3C216	J2003-3251	C	1	2000-330
J0920+4441	C	1	0917+449	J2005+7752	C	4	2007+777
J0927+3902	L	1	0923+392 4C39.25	J2022+6136	C	1	2021+614
J0927+3902	C	1	0923+392 4C39.25	J2129-1538	L	1	2126-158
J0948+4039	C	1	0945+408	J2129-1538	C	1	2126-158
J0953+0755	L	1	PSR0950+08	J2136+0041	C	1	2134+004
J0955+6903	L	1	0951+693 M81	J2157-6941	C	1	2152-699
J0955+6903	C	1	0951+693 M81	J2158-3013	L	1	2155-304
J0958+6533	L	1	0954+658	J2202+4216	C	1	2200+420 BLLac
J0958+6533	C	3	0954+658	J2217+0220	L	1	2215+020
J1015+4925	C	1	1011+496	J2225-0457	L	1	2223-052 3C446
J1041+5233	L	1	1038+52C	J2225-0457	C	1	2223-052 3C446
J1041+5233	C	1	1038+52C	J2232+1143	C	1	2230+114 CTA102
J1042+1203	C	1	1040+123 3C245	J2253+1608	L	1	2251+158 3C454.3
J1104+3812	C	1	1104+382 Mkn421	J2253+1608	C	1	2251+158 3C454.3
J1130-1449	L	1	1127-145	J2256+6201	L	1	CepA
J1139+6547	C	1	1137+660 3C263	J2338+2701	C	1	2335+267 3C465

10.2 5 GHz VLBA Continuum Survey

Table 13 contain data on 377 out of a complete sample of 379 continuum extragalactic sources observed with VLBA in June 1996. The sources 0413+111 and 2145-153 met the sample criteria but were not observed and are not listed in the table There are redshifts, obtained from NED, for 322 of the sources. For sources with velocities less than 10,000 km/s, NED supplies a velocity instead of a redshift and the redshift in the tables is simply this velocity divided by the speed of light. These redshifts should therefore be treated with caution. The S_5 and S_{120} values are the correlated flux at 5- and 120-Mega-wavelengths respectively. The source classification is again from NED: G = Galaxy, VisS = Visual Source (with no known redshift), etc. The rest are self-explanatory. The 'other name' column contains common names for the sources.

11 VSOP Scheduling Process

11.1 Differences Between VSOP and Other Space Astronomy Missions

Unlike most space astronomy missions, the VSOP mission *requires* co-observing ground telescopes to obtain any useful scientific data. The space VLBI mission has obtained commitments of time from ground radio observatories. However, because these do not cover 100% of the possible VSOP observing time and all possible requests from proposers, they constitute another mission constraint which must be taken into account in the scheduling process.

11.2 Ground Radio Telescopes Availability

Table 6 lists the ground radio telescopes (GRTs) expected to support space VLBI observations along with their SEFD values at the VSOP observing frequencies (as expected in early 1999) and the percentage of the time that these telescopes have committed to space VLBI. All ten VLBA telescopes are schedules as a single unit. This also is true of the EVN as a whole for 15% of the time (half the EVN network time), but some individual telescopes in the EVN are available another 5–15% of the time. Each of the remaining telescopes in Table 6 has been committed only individually, but can be gathered into an *ad hoc* array depending on availability.

11.3 Differences Between VSOP and Ground VLBI Scheduling

The scheduling of VLBI experiments with the VSOP mission is performed by the VSOG. Unlike ground VLBI experiments, the (u,v) coverage attainable for a particular source can vary greatly from month to month. Because of the large solar avoidance regions and the telemetry antenna horizon mask, certain regions of the sky are unobservable for periods of up to 5 months. Even when a source is observable, because of the orbital precession, the (u,v) coverage attainable could be somewhat foreshortened or even one-dimensional at certain times. This may or may not be acceptable for a particular science program.

To find the best period in which to observe a source the scheduler must search over many possible observing slots — 15 months for AO phase 2 observations (Oct 1998-Dec 1999) — to determine when the preferred (u,v) coverage occurs (Although AO observations nominally begin in Jan 1999 some AO2 observations may be scheduled as early as Oct 1998 if the best (u,v) coverage for these observations occurs at this epoch).

Performing this for each source in each program results in having to schedule many hundreds of observations for each AO phase. In this process a proposer may not receive the preferred (u,v) coverage (see below for more details).

11.4 VSOP Scheduling Process

As with most other open-proposal observatories, the likelihood of an observing program receiving its requested resources is determined by the scientific value of the program and the availability of the resources

Table 13: 5 GHz VLBA Survey

J2000 name	B1950 name	S_5	S_{120}	ID	z	other name	J2000 name	B1950 name	S_5	S_{120}	ID	z	other name
J0006−06	0003−066	3.0	1.5	G	0.347		J0522−36	0521−365	2.6	1.0	G	0.055	
J0013+40	0010+405	0.7	0.3	G	0.255		J0530+13	0528+134	7.8	5.3	QSO	2.060	
J0019+73	0016+731	1.6	1.2	QSO	1.781		J0530−25	0528−250	1.1	0.3	QSO	2.779	
J0029+34	0026+346	1.4	<0.2	G	0.600	0025+345	J0532+07	0529+075	2.5	<0.2	RadioS	–	
J0038+41	0035+413	0.7	<0.2	QSO	1.353		J0539−28	0537−286	0.6	0.4	QSO	3.104	
J0042+23	0039+230	1.2	0.4	RadioS	–		J0541−05	0539−057	1.5	0.6	QSO	0.839	
J0050−09	0048−097	1.5	1.5	BLL	–		J0542+49	0538+498	2.6	0.5	QSO	0.545	3C147
J0057+30	0055+300	0.9	<0.2	G	0.016		J0555+39	0552+398	7.9	4.5	QSO	2.365	DA193
J0059+00	0056−001	1.2	0.2	QSO	0.717		J0604−31	0602−319	<0.2	<0.2	QSO	0.452	
J0105+48	0102+480	1.4	0.8	RadioS	–		J0607+67	0602+673	1.0	1.0	QSO	–	
J0106−40	0104−408	3.0	2.0	QSO	0.584		J0607−08	0605−085	3.0	1.8	QSO	0.870	
J0108+01	0106+013	2.0	0.5	QSO	2.099		J0608−22	0606−223	0.7	0.7	QSO	1.926	
J0111+39	0108+388	1.6	0.2	G	0.669		J0609−15	0607−157	5.2	3.5	QSO	0.324	
J0115−01	0112−017	1.4	0.5	QSO	1.365		J0614+60	0609+607	1.2	0.9	QSO	2.690	
J0116−11	0113−118	1.4	0.6	QSO	0.672		J0616−34	0614−349	<0.2	<0.2	GPair	0.329	
J0119+08	0116+082	0.6	<0.2	G	0.593		J0620−37	0618−371	0.2	<0.2	GPair	0.032	
J0119+32	0116+319	0.9	<0.2	GPair	0.059		J0626+82	0615+820	1.0	0.5	QSO	0.710	
J0120−27	0118−272	1.0	0.3	BLL	0.559		J0627−05	0624−058	<0.2	<0.2	RadioS	–	
J0121+04	0119+041	1.7	1.0	QSO	0.637		J0627−35	0625−354	0.9	<0.2	G	0.054	
J0121+11	0119+115	1.4	1.4	G	0.570		J0636−20	0634−205	<0.2	<0.2	G	0.056	
J0125−00	0122−003	2.0	0.5	QSO	1.070		J0644−34	0642−349	1.2	0.5	QSO	2.165	
J0126+25	0123+257	1.0	1.0	QSO	2.358		J0646+44	0642+449	2.1	1.9	QSO	3.396	
J0126−01	0123−016	<0.2	<0.2	RadioS	–		J0648−30	0646−306	1.0	0.6	QSO	0.455	
J0132−16	0130−171	1.5	0.7	QSO	1.022		J0648−39	0646−398	0.2	<0.2	RadioS	–	
J0134−36	0132−363	<0.2	<0.2	G	0.015		J0710+47	0707+476	0.9	0.9	QSO	1.292	
J0136+47	0133+476	3.0	3.0	QSO	0.859	DA55	J0713+43	0710+439	1.8	0.5	QSO	0.518	
J0137+33	0134+329	0.7	<0.2	QSO	0.367	3C48	J0714+35	0711+356	1.3	1.0	QSO	1.620	
J0137−24	0135−247	1.5	1.3	QSO	0.831		J0721+71	0716+714	0.3	0.3	BLL	–	
J0140+08	0137+085	<0.2	<0.2	RadioS	–		J0738+17	0735+178	1.8	0.3	BLL	–	
J0141−09	0138−097	0.7	0.4	BLL	0.440		J0739+01	0736+017	2.2	1.1	QSO	0.191	
J0149+05	0146+056	1.7	0.8	QSO	2.345		J0741+31	0738+313	4.2	2.0	QSO	0.635	
J0152+22	0149+218	1.4	1.4	QSO	1.320		J0745+10	0742+103	4.2	1.5	RadioS	–	
J0153−33	0150−334	1.1	0.3	QSO	0.610		J0745−00	0743−006	2.5	1.2	BLL	0.994	
J0155−40	0153−410	1.1	0.2	G	–		J0748+24	0745+241	1.0	0.7	QSO	0.410	
J0157+74	0153+744	1.6	<0.2	QSO	2.338		J0750+12	0748+126	2.4	1.7	QSO	0.889	
J0204+15	0202+149	3.1	2.5	QSO	–		J0758+37	0755+379	0.3	<0.2	G	0.043	
J0204−17	0202−172	1.5	1.0	QSO	1.740		J0808+49	0804+499	1.3	1.0	QSO	1.430	
J0205+32	0202+319	1.0	0.7	QSO	1.466		J0808−07	0805−077	1.2	0.3	QSO	1.837	
J0217+01	0215+015	1.2	1.1	BLL	1.715		J0811+01	0808+019	1.6	1.6	BLL	–	
J0217+73	0212+735	4.0	2.7	BLL	2.367		J0815+36	0812+367	1.2	1.2	QSO	1.025	
J0221+35	0218+357	1.1	<0.2	BLL	0.684		J0818+42	0814+425	1.4	0.5	BLL	0.025	
J0224+06	0221+067	0.8	0.6	QSO	0.511		J0820−12	0818−128	0.6	0.4	BLL	–	
J0226+34	0223+341	1.3	0.4	QSO	–		J0823+22	0820+225	1.5	0.3	BLL	0.951	
J0231+13	0229+131	1.7	1.1	G	2.059		J0824+39	0821+394	1.2	1.2	QSO	1.216	
J0237+28	0234+285	2.5	1.5	QSO	1.213		J0824+55	0820+560	1.3	0.8	QSO	1.417	
J0238+16	0235+164	0.6	0.3	BLL	0.940		J0825+03	0823+033	2.0	1.7	BLL	0.506	
J0239+04	0237+040	1.1	0.7	QSO	0.978		J0831+04	0829+046	1.4	0.5	BLL	0.180	
J0240−23	0237−233	3.5	<0.2	QSO	2.223		J0832+49	0828+493	0.4	0.3	BLL	0.548	
J0241−08	0238−084	3.1	0.2	G	0.004	NGC1052	J0834+55	0831+557	6.0	0.5	G	0.242	
J0242+11	0239+108	2.0	1.0	QSO	–		J0836−20	0834−201	3.3	1.7	QSO	2.752	
J0251+43	0248+430	1.6	0.5	QSO	1.310		J0837+58	0833+585	0.7	0.2	QSO	2.101	
J0259+07	0256+075	0.9	0.7	BLL	0.893		J0840+13	0838+133	0.7	0.5	QSO	0.684	
J0312+01	0310+013	0.5	0.5	QSO	0.664		J0841+70	0836+710	2.5	0.5	QSO	2.172	
J0318+41	0314+416	<0.2	<0.2	G	0.025		J0842+18	0839+187	1.2	0.4	QSO	1.270	
J0319+41	0316+413	30.0	2.0	G	0.017	3C84	J0854+20	0851+202	1.9	1.1	BLL	0.306	OJ287
J0321+12	0319+121	1.2	1.0	QSO	2.662		J0854+57	0850+581	1.1	0.9	QSO	1.322	
J0322−37	0320−373	<0.2	<0.2	G	0.005	FOR-A	J0900−28	0858−279	4.5	<0.2	QSO	2.152	
J0334+08	0332+078	0.6	0.6	VisS	–		J0903+46	0859+470	1.0	0.7	QSO	1.462	
J0334−40	0332−403	2.6	2.3	QSO	1.445		J0909+01	0906+015	0.6	0.4	QSO	1.018	
J0336+32	0333+321	2.2	0.6	QSO	1.258	NRAO140	J0909+42	0906+432	0.8	0.7	QSO	0.670	0906+430
J0339−01	0336−019	2.5	0.8	QSO	0.852	CTA26	J0920+44	0917+449	1.5	1.3	QSO	2.180	
J0348−27	0346−279	1.5	1.1	QSO	0.988		J0921+62	0917+624	1.9	1.7	QSO	1.446	
J0359+50	0355+508	2.0	0.4	QSO	–	NRAO150	J0921−26	0919−260	1.8	0.4	QSO	2.300	
J0402−31	0400−319	0.9	0.4	QSO	–		J0927+39	0923+392	14.0	9.0	QSO	0.699	4C39.25
J0403+26	0400+258	1.0	0.5	QSO	2.109		J0948+40	0945+408	2.0	1.8	QSO	1.252	
J0403−36	0402−362	2.7	2.7	QSO	1.417		J0949+66	0945+664	<0.2	<0.2	VisS	–	
J0405+38	0402+379	0.8	<0.2	G	0.055		J0956+25	0953+254	1.6	0.6	QSO	0.712	OK290
J0405−13	0403−132	1.0	1.0	QSO	0.571		J0957+55	0954+556	0.9	<0.2	QSO	0.909	4C55.17
J0406−38	0405−385	1.6	1.5	QSO	1.285		J0958+47	0955+476	1.6	1.6	QSO	1.873	
J0407−12	0405−123	0.8	0.6	QSO	0.574		J0958+65	0954+658	0.9	0.9	BLL	0.368	
J0412+23	0409+229	0.4	<0.2	QSO	1.215		J1006+34	1003+351	0.3	<0.2	G	0.098	3C236
J0414+05	0411+054	0.3	<0.2	QSO	2.639		J1014+23	1012+232	1.0	0.7	QSO	0.565	
J0414+34	0411+341	2.0	<0.2	RadioS	–		J1018−31	1015−314	0.7	<0.2	QSO	1.346	
J0416−18	0414−189	1.5	1.3	QSO	1.536		J1033+41	1030+415	0.3	0.3	QSO	1.120	
J0418+38	0415+379	1.5	<0.2	G	0.048		J1035+56	1031+567	1.6	0.3	G	0.450	
J0423−01	0420−014	3.8	2.5	QSO	0.915		J1035−20	1032−199	0.8	0.5	QSO	2.189	
J0424+00	0422+004	0.6	0.5	BLL	0.310		J1037−29	1034−293	2.0	1.8	BLL	0.312	
J0424−37	0422−380	1.5	0.8	QSO	0.782		J1041+02	1039+029	<0.2	<0.2	RadioS	–	
J0428−37	0426−380	2.2	1.8	BLL	1.030		J1041+06	1038+064	2.1	1.8	QSO	1.270	
J0431+20	0428+205	2.1	<0.2	G	0.219		J1042+12	1040+123	0.7	0.3	QSO	1.029	3C245
J0433+05	0430+052	4.0	0.5	G	0.032	3C120	J1044+80	1039+811	0.9	0.5	QSO	1.260	
J0437+29	0433+295	0.2	<0.2	G	0.217	3C123	J1048+71	1044+719	1.8	1.8	QSO	1.150	
J0437−18	0434−188	1.3	0.6	QSO	2.702		J1048−19	1045−188	1.1	1.1	QSO	0.595	
J0440−43	0438−436	2.5	1.2	QSO	2.852		J1048−41	1046−409	0.4	0.2	QSO	0.620	
J0442−00	0440−003	1.9	0.6	QSO	0.844	NRAO190	J1051+21	1049+215	1.6	0.9	QSO	1.300	
J0449+11	0446+112	1.2	0.6	G	1.207		J1051−31	1048−313	1.2	0.7	RadioS	–	
J0453−28	0451−282	2.5	0.5	QSO	2.559		J1058+01	1055+018	3.5	1.7	BLL	0.888	
J0455−30	0453−301	<0.2	<0.2	G	–		J1058+19	1055+201	0.6	0.5	QSO	1.110	
J0457−23	0454−234	2.1	1.4	BLL	1.009		J1118+12	1116+128	1.6	0.8	QSO	2.118	
J0459+02	0457+024	2.1	0.4	QSO	2.384		J1125+26	1123+264	1.3	1.2	QSO	2.341	
J0501−01	0458−020	2.6	1.3	QSO	2.286		J1127−18	1124−186	1.4	1.4	QSO	1.050	
J0503+02	0500+019	2.6	0.8	QSO	1.000		J1130−14	1127−145	4.5	0.8	QSO	1.187	
J0508+84	0454+844	0.5	0.5	BLL	0.112		J1139−13	1136−135	0.3	<0.2	QSO	0.554	
J0509+05	0506+056	0.6	0.5	VisS	–		J1146−24	1143−245	1.7	0.9	QSO	1.950	
J0513−21	0511−220	0.9	0.4	QSO	1.296		J1146−33	1143−331	0.3	<0.2	G	–	

Table 13: 5 GHz VLBA Survey (*continued*)

J2000 name	B1950 name	S_5	S_{120}	ID	z	other name
J1147−07	1145−071	1.1	0.7	QSO	1.342	
J1147−38	1144−379	2.5	1.5	BLL	1.048	
J1150+24	1147+245	0.8	0.5	BLL	–	
J1150−00	1148−001	1.8	0.4	QSO	1.976	
J1153+49	1150+497	1.2	0.9	QSO	0.334	
J1153+80	1150+812	1.7	1.3	QSO	1.250	
J1158+24	1155+251	1.0	0.2	G	–	
J1159+29	1156+295	2.2	2.2	QSO	0.729	
J1205−26	1203−262	0.4	0.4	QSO	0.789	1202-262
J1209−24	1206−238	0.9	0.4	QSO	–	
J1215+34	1213+350	1.0	0.3	QSO	0.857	
J1215−17	1213−172	2.2	2.2	G	–	
J1219+48	1216+487	1.1	0.7	QSO	1.076	
J1224+03	1222+037	1.3	0.7	QSO	0.957	
J1224+21	1222+216	1.8	1.8	QSO	0.435	
J1225+12	1222+131	0.3	0.2	G	0.003	3C272.1
J1229+02	1226+023	4.0	1.0	QSO	0.158	3C273B
J1230+12	1228+126	3.5	0.6	G	0.004	3C274
J1232−02	1229−021	0.8	0.3	QSO	1.045	
J1239−10	1237−101	1.6	0.3	QSO	0.753	
J1242−04	1239−044	<0.2	<0.2	G	0.480	
J1246−07	1243−072	1.1	0.8	QSO	1.286	
J1246−25	1244−255	1.4	0.6	QSO	0.638	
J1254+11	1252+119	0.9	0.4	QSO	0.871	
J1256−05	1253−055	13.0	2.5	QSO	0.538	3C279
J1257−31	1255−316	1.7	1.3	QSO	1.924	
J1305−10	1302−102	1.0	0.4	QSO	0.286	
J1309+11	1307+121	0.9	0.4	BLL	–	
J1310+32	1308+326	4.5	3.6	BLL	0.996	
J1316−33	1313−333	2.0	1.2	QSO	1.210	
J1325−43	1322−427	4.7	<0.2	G	0.001	CEN-A
J1331+30	1328+307	4.2	<0.2	QSO	0.849	3C286
J1332+02	1330+022	0.6	0.3	G	0.216	
J1337−12	1334−127	5.5	5.0	BLL	0.539	
J1347+12	1345+125	1.6	0.3	G	0.120	
J1351−14	1349−145	0.7	0.5	RadioS	–	
J1354−10	1352−104	0.6	0.3	QSO	0.332	
J1357+19	1354+195	1.3	0.5	QSO	0.720	
J1357−15	1354−152	0.8	0.7	QSO	1.890	
J1357−17	1354−174	1.4	0.5	G	3.147	
J1405+04	1402+044	1.1	1.1	QSO	3.193	
J1407+28	1404+286	3.0	1.0	G	0.076	OQ208
J1408−07	1406−076	0.9	0.8	QSO	1.494	
J1411+52	1409+524	<0.2	<0.2	G	0.460	3C295
J1415+13	1413+135	1.1	1.1	BLL	0.260	
J1419+54	1418+546	0.8	0.3	BLL	0.152	
J1419−19	1417−192	0.5	0.4	G	0.119	
J1427−42	1424−418	4.2	3.7	QSO	1.522	
J1430+10	1427+109	1.3	1.2	QSO	1.710	
J1436+63	1435+638	1.4	0.5	QSO	2.068	
J1445+09	1442+101	1.2	0.2	QSO	3.522	
J1454−37	1451−375	3.0	2.2	QSO	0.314	
J1501−39	1458−391	1.2	<0.2	RadioS	–	
J1504+10	1502+106	2.2	1.2	QSO	1.839	
J1506+37	1504+377	1.1	1.0	G	0.674	
J1507−16	1504−166	3.0	1.2	QSO	0.876	
J1510−05	1508−055	0.7	0.7	QSO	1.185	
J1512−09	1510−089	2.8	1.5	QSO	0.360	
J1513−10	1511−100	1.1	0.7	QSO	1.513	
J1516+00	1514+004	1.1	1.0	G	0.052	
J1517−24	1514−241	2.8	1.5	G	0.042	
J1522−27	1519−273	2.2	2.2	BLL	–	
J1526−13	1524−136	1.0	<0.2	QSO	1.687	
J1530−42	1526−423	<0.2	<0.2	RadioS	–	
J1534+01	1532+016	1.3	0.3	QSO	1.435	
J1540+14	1538+149	1.1	1.0	BLL	0.605	
J1543−07	1540−077	1.1	<0.2	G	–	
J1546+00	1543+005	1.2	0.4	G	0.550	
J1549+02	1546+027	1.9	1.9	QSO	0.413	
J1550+05	1548+056	3.5	3.0	QSO	1.422	
J1554−27	1550−269	0.6	<0.2	QSO	2.145	
J1557−00	1555+001	1.4	1.2	QSO	1.770	
J1602+33	1600+335	2.2	1.4	G	–	
J1608+10	1606+106	1.6	0.8	QSO	1.226	
J1613+34	1611+343	5.0	2.5	QSO	1.401	
J1625+41	1624+416	1.3	0.2	QSO	2.550	
J1625−25	1622−253	4.2	3.8	G	0.786	
J1626−29	1622−297	3.0	1.5	QSO	0.815	
J1632+82	1637+826	0.7	0.2	G	0.023	
J1635+38	1633+382	2.7	0.5	QSO	1.814	
J1637+47	1636+473	1.0	0.5	QSO	0.740	
J1638+57	1637+574	1.6	1.5	QSO	0.745	
J1640+12	1638+124	0.9	0.4	G	–	
J1640+39	1638+398	1.0	0.7	QSO	1.660	NRAO512
J1642+39	1641+399	7.6	2.0	QSO	0.593	3C345
J1642+68	1642+690	1.3	0.7	QSO	0.751	
J1642−06	1639−062	2.0	<0.2	RadioS	–	
J1651+01	1648+015	0.9	0.9	VisS	–	
J1651+04	1648+050	<0.2	<0.2	G	0.154	3C348
J1653+39	1652+398	1.0	0.5	BLL	0.033	DA426
J1658+05	1656+053	1.3	0.7	QSO	0.879	
J1658+07	1655+077	1.3	0.8	QSO	0.621	
J1658+47	1656+477	1.0	0.9	QSO	1.622	
J1720−00	1717−009	<0.2	<0.2	G	0.030	3C353
J1724−02	1721−026	<0.2	<0.2	RadioS	–	
J1727+45	1726+455	1.6	1.2	QSO	0.714	
J1728+04	1725+044	0.8	0.3	QSO	0.296	
J1733−13	1730−130	8.0	6.0	QSO	0.902	NRAO530
J1734+38	1732+389	1.6	1.2	BLL	0.970	
J1740+52	1739+522	1.1	1.0	QSO	1.375	
J1743−03	1741−038	3.0	2.0	QSO	1.054	
J1745−07	1742−078	1.4	<0.2	RadioS	–	
J1748+70	1749+701	0.8	0.3	BLL	0.770	
J1751+09	1749+096	1.0	1.0	BLL	0.322	
J1753+44	1751+441	0.7	0.4	QSO	0.871	
J1800+78	1803+784	3.3	2.4	BLL	0.680	
J1801+44	1800+440	0.7	0.7	QSO	0.663	
J1804+01	1801+010	1.0	<0.2	QSO	1.522	
J1806+69	1807+698	1.5	0.4	BLL	0.051	3C371
J1824+10	1821+107	<0.2	<0.2	QSO	1.360	
J1824+56	1823+568	1.9	1.9	BLL	0.664	
J1832+28	1830+285	0.7	0.5	QSO	0.594	
J1833−21	1830−211	3.6	<0.2	QSO	–	
J1842+79	1845+797	1.0	0.4	G	0.056	
J1902+31	1901+319	1.6	0.4	QSO	0.635	3C395
J1911−20	1908−201	2.2	1.0	RadioS	–	
J1924−29	1921−293	18.5	9.5	QSO	0.352	
J1925+21	1923+210	1.5	0.5	RadioS	–	
J1927+73	1928+738	4.0	1.5	QSO	0.302	
J1937−39	1933−400	1.4	0.8	QSO	0.966	
J1939−15	1936−155	1.8	1.8	QSO	1.657	
J1949−19	1946−200	1.4	<0.2	RadioS	–	
J1955+51	1954+513	2.0	0.3	QSO	1.220	
J1957−38	1954−388	5.5	5.0	QSO	0.630	
J1959+40	1957+405	1.0	0.2	GPair	0.056	CYG-A
J2000−17	1958−179	2.2	2.2	QSO	0.650	
J2003−32	2000−330	1.3	0.5	QSO	3.773	
J2005+77	2007+777	1.4	0.8	BLL	0.342	
J2011−15	2008−159	1.6	1.6	QSO	1.180	
J2022+61	2021+614	3.8	1.2	QSO	0.227	
J2031+12	2029+121	1.3	0.9	BLL	1.215	
J2040−25	2037−253	0.6	0.5	QSO	1.574	
J2101+03	2059+034	1.2	0.4	QSO	1.013	
J2109−41	2106−413	2.7	1.5	QSO	1.055	
J2110−10	2107−105	1.2	0.5	QSO	–	
J2115+29	2113+293	1.0	0.3	QSO	1.514	
J2123+05	2121+053	0.8	0.5	QSO	1.878	
J2129−15	2126−158	1.4	0.4	QSO	3.268	
J2131−12	2128−123	2.8	0.3	QSO	0.501	
J2134−01	2131−021	1.8	0.4	BLL	0.557	
J2136+00	2134+004	11.0	1.0	QSO	1.932	
J2139+14	2136+141	2.5	0.6	QSO	2.427	
J2147+09	2144+092	1.1	0.4	QSO	1.113	
J2148+06	2145+067	8.0	3.0	QSO	0.990	
J2151+05	2149+056	1.1	0.4	G	0.740	
J2151−30	2149−307	1.8	0.3	QSO	2.345	2149-306
J2152+17	2150+173	0.7	0.2	BLL	–	
J2158−15	2155−152	3.0	0.5	BLL	0.672	
J2202+42	2200+420	7.0	1.0	BLL	0.068	BL-LAC
J2203+31	2201+315	2.6	0.3	QSO	0.301	
J2206−18	2203−188	0.4	<0.2	QSO	0.620	
J2209−23	2206−237	<0.2	<0.2	G	0.087	
J2212+23	2209+236	1.8	0.4	QSO	–	
J2213−25	2210−257	0.9	0.2	QSO	1.833	
J2218−03	2216−038	3.0	0.6	QSO	0.901	
J2225+21	2223+210	0.8	<0.2	QSO	1.959	
J2225−04	2223−052	3.0	0.6	BLL	1.404	3C446
J2229−08	2227−088	1.8	1.0	QSO	1.561	
J2230+69	2229+695	0.5	<0.2	G	–	
J2230−39	2227−399	0.5	0.3	QSO	0.323	
J2232+11	2230+114	5.5	0.4	QSO	1.037	CTA102
J2236+28	2234+282	1.4	0.4	QSO	0.795	
J2243−25	2240−260	0.3	<0.2	BLL	0.774	
J2246−12	2243−123	2.6	0.9	QSO	0.630	
J2248−32	2245−328	0.7	0.3	QSO	2.268	
J2249+11	2247+113	<0.2	<0.2	G	0.026	
J2250+14	2247+140	<0.2	<0.2	QSO	0.237	
J2253+16	2251+158	20.0	6.0	QSO	0.859	3C454.3
J2255+42	2253+417	1.1	0.3	QSO	1.476	
J2256−36	2254−368	<0.2	<0.2	G	0.006	
J2257+07	2254+074	0.6	0.2	BLL	0.190	
J2258−27	2255−282	2.8	2.2	QSO	0.926	
J2311+34	2308+341	0.9	0.3	QSO	1.817	
J2320+05	2318+049	1.1	0.8	QSO	0.623	
J2321+27	2319+272	1.0	0.3	QSO	1.253	
J2330+11	2328+107	1.5	0.3	QSO	1.489	
J2331−15	2329−162	1.5	0.6	QSO	1.155	
J2333−23	2331−240	0.9	0.2	G	0.047	
J2339−33	2337−334	0.7	<0.2	RadioS	–	
J2346+09	2344+092	1.6	0.3	QSO	0.677	
J2348−16	2345−167	3.2	1.6	QSO	0.576	
J2354+45	2351+456	1.5	0.3	QSO	1.992	
J2355+49	2352+495	1.5	0.2	G	0.237	
J2357−11	2354−117	1.7	0.3	QSO	0.960	2354-116
J2358−10	2355−106	1.8	1.8	QSO	1.626	

it requires. The first step in this process is an evaluation of each proposal by an independent and international Science Review Committee (SRC). In addition, in consultation with a technical review by the VSOG, the SRC may recommend an increase or decrease in the amount of observing time and ground facilities an observation needs to accomplish its stated scientific goals. After the evaluation process is complete, the VSOG begins to schedule observations in proposal ranking order (highest ranked proposals first) throughout the AO period until all the available resources are used up. Some amount of schedule shifting is employed to allow as many highly-ranked programs as possible to be scheduled. This may result in many programs having (u,v) coverage that is not as good as the proposer desires in the effort to optimally allocate all the highly rated scientific programs.

Currently about 45% of the in-orbit time is used for scientific observations. This limit is caused by the large amount of time needed to maneuver the spacecraft between sources and re-establish the pointing. The result of the scheduling effort will be a "long-term" schedule over the entire AO phase 2 observing period. It will be used to periodically generate "detailed" schedules of one month duration. Re-generation of the long-term schedule sometimes will be necessary to take into account un-modeled orbital evolution or changes in the spacecraft, mission capabilities, or GRT commitments. However, as the general orbital plane precession is well known, the time of year when a source is best observed will remain about the same.

11.5 Requesting Specific GRTs

A proposer may suggest a specific array of co-observing GRTs or leave this choice to the VSOG. In the latter case, an array will be chosen for the experiment based on the scientific goals, the proposal's scientific ranking by the SRC, the availability of the GRTs, and the source declination. For northern hemisphere sources, observations generally are performed with HALCA and either the EVN or the VLBA alone. Sometimes one or more large telescopes are used to augment the VLBA to enhance fringe finding on weaker sources. On rare occasions, a particularly highly-ranked experiment may employ both the EVN and VLBA, plus additional large GRTs, in order to obtain dense, sensitive (u,v) coverage. For sources in the deep south, a southern hemisphere VLBI array is used, composed of telescopes in Australia and South Africa. For equatorial sources, the arrays are more *ad hoc*, involving telescopes chosen from both northern and southern arrays, based on the declination of the source and telescope availability. If proposers want to use the EVN array without the VLBA then the EVN must be augmented with 'outrigger' telescopes such as Usuda 64m telescope (UD) or the Green Bank 43m telescope (GB) to obtain good (u,v) coverage with HALCA.

Many proposers choose to suggest one of the above options in the "Additional notes to the scheduler" section on the proposal cover sheet in order to assist the VSOG in determining what kind of array the proposer needs. In this case, the VSOG will make every effort to schedule the suggested array, or one that is similar, based on proposal ranking and array availability. However, because the best time to observe a source and the availability of the requested array sometimes may not be compatible, it will not be possible always to schedule the exact array requested.

Sometimes the scientific goals of the experiment (*e.g.*, very sensitive observations or polarization experiments) demand the use of specific telescopes. In that case, the proposer *must* specify the telescopes requested and clearly state in the scientific and technical justification section of the proposal why these unique facilities are needed. When such experiments are scheduled, availability of the resources will be the primary factor determining the observing date, while (u,v) coverage will be a secondary factor.

11.6 Interface Between Proposers and the VSOP Scheduling Process

Because the scheduling process is complex, the schedulers will have little time for detailed and frequent interactions with the proposers. Personal or e-mail interactions usually are scheduler-initiated. The first and foremost interaction with the scheduler is through the proposal Cover Sheets and the scientific and technical justification. These have been designed to give the proposer some ability to control the scheduling process before it begins. Some of the crucial items are the suggested GRT array (discussed above) and, for monitoring programs, the preferred number of observations and their mean interval spacing.

Once the long-term schedule has been generated, the PI (or designated contact person) will be notified by the VSOG of the tentative date(s) on which their observation(s) has (have) been tentatively scheduled. If this is significantly in the future, there is a finite chance that the scheduled date may change in the intervening time. Once a detailed schedule for the observation has been created, and a firm observing date determined, the PI will again be notified by the VSOG.

If information on the Cover Sheets changes in the interval between writing the proposal and scheduling the observation (*e.g.*, the date of simultaneous observation with optical or X-ray telescopes), these facts must be transmitted as soon as possible to the VSOG by e-mail (vsog@vsop.isas.ac.jp).

12 HALCA Calibration

Proposers should be aware of the general VLBI calibration scheme for HALCA and the types of data products that the VSOG will make available for *a priori* calibration of their space VLBI data. The two types of *a priori* calibration are amplitude calibration and (inter-channel) phase calibration. (The details of instrumental polarization calibration of HALCA, necessary for linear polarization observations, are discussed in §9.10.) The VSOG also expects to make some *a priori* flagging data available.

12.1 Amplitude Calibration

Since information about the relative strength of the electro-magnetic wave originating at the radio-source and arriving at each telescope is lost when the signal is added to the system noise and then digitized and sampled, a measure of the relative system noise power at each telescope is necessary to properly scale the correlation coefficients obtained at the correlator to sensible astronomical units, i.e., flux density (Jy). This is achieved by measuring the so-called System Equivalent Flux Density (SEFD) of each telescope during the VLBI observations. The SEFD, which completely describes the sensitivity of an antenna-receiver system to weak radio-sources, is the ratio of the system temperature and the antenna sensitivity.

The system temperature of a radio telescope is an absolute measure of the noise power generated by the 'system' which obscures the desired radio-source signal. For ground radio telescopes, the system temperature consists principally of the noise power contributed by the receiver electronics, except at higher radio frequencies where water vapor in the atmosphere becomes an significant component. System temperature is usually monitored as a function of elevation and time. For HALCA, the system temperature is a function of several observing conditions. The physical temperature of various science subsystem components determines the noise contribution of both the receiver and system temperature calibration electronics. Thus, the system temperature depends on the the sun angle and after maneuvering, it typically varies monotonically by $\sim$10% over several orbits as the spacecraft acclimates to the new heating profile. In addition, re-acclimation after each eclipse occurs within a period a few times the length of the eclipse and may cause system temperature variations of a few percent. Finally, near perigee, the presence of the Earth in the antenna side-lobes can add 10–30% to the system temperature (and potentially much more, but the Ku-band telemetry link, and therefore VLBI observing, is usually not possible when the earth is nearer the pointing direction). The largest and most rapid system temperature variations occur near perigee.

System temperature is typically measured by synchronously detecting and comparing an injected noise source of known power to the system noise power. Unlike many ground radio telescopes, HALCA does not have the ability to measure system temperature continuously during VLBI recording due to the limited on-board spacecraft command memory. During the In-Orbit-Checkout and first months of General Observing, the system temperature has typically been measured when the measurement system can be turned on for long periods, e.g., during the first orbit after arriving on-source, just before maneuvering to the next, and during periods otherwise not allocated for VLBI. These measurements are then interpolated to cover the VLBI recording time ranges. In general, this has been sufficient to characterize the most significant system temperature variations; indeed, HALCA's system temperature tends to be more stable than that of typical ground radio telescopes owing to the homogeneity of the orbiting environment, in particular, lack of atmosphere and ground pickup. One possible exception is radio-frequency interference (RFI) in the 1.6 GHz band which has been observed sporadically at as much as the 30% level (and not necessarily in the direction of the Earth–geostationary satellites are a suspected source of RFI). For observations where it is not possible to make the measurements in this manner, it is probable that some system temperature measurements will be made for short (< a few minutes) intervals during VLBI recording. In this case, since the injected noise source approximately doubles the system temperature (50% duty cycle) the VLBI data obtained during the measurement will probably be unusable.

The antenna sensitivity is a measure of the radio telescope's response to weak signals and for ground radio telescopes, its nominal magnitude depends principally on the size of the antenna's aperture and the quality of its surface, the traditional aperture efficiency. It is normally a variable function of only pointing accuracy and the source elevation (via differential gravitational loading on the antenna structure and at higher radio frequencies, atmospheric attenuation by water vapor); thus the antenna pointing must be verified and a gain–elevation curve measured in convenient units, usually degrees Kelvin of system temperature added per Jansky of radio-source emission.

For HALCA, there are additional design-dependent components to the nominal antenna sensitivity (e.g., feed and cable losses, see §3). The variable component is also somewhat more complicated. The shape and efficiency of the mesh surface depends on differential heating by the Sun and thus the gain and pointing accuracy are functions of sun angle. Furthermore, HALCA experiences eclipses of variable length and it is likely that this imparts additional variations. HALCA's antenna sensitivity and pointing accuracy are measured periodically by bore-sight calibration (observing system temperature variations with pointing offsets) using strong (> 500 Jy) and compact continuum sources at both HALCA frequencies. With the current sun angle and maneuvering constraints and the limited number of suitable radio sources, the complete description of the dependence on sun angle and eclipse history is not yet available. The pointing accuracy of HALCA has been observed to be better than $\sim$2 minutes of arc, and typical values of antenna sensitivity (in units of mK/Jy), from measurements made in October and November 1997 are given in Table 1. Although some degradation at 1.6 GHz has occurred during the In-Orbit Checkout period, it is thought that the system gain is known to within 10-15%, and is considerably more stable than this over the duration of a typical observation.

It will be the responsibility of the VSOG and NOT the PI to determine and implement the amplitude calibration scheme for a particular observation. Any non-standard requirements of a particular experiment *must* be specified in the proposal Cover Sheets and justified in the technical and scientific justification. Since HALCA differs significantly from ground radio telescopes in the details and difficulties of its amplitude calibration scheme, proposers are cautioned against making direct comparisons of HALCA to ground radio telescopes via the individual measures of system performance listed in Table 1, especially 'aperture' efficiency. Considered separately, quantities such as system temperature, antenna sensitivity, and aperture efficiency depend critically upon the location of the system calibration reference point, which for HALCA is located approximately at the LNA input and *behind* the feed and cable losses described in §3. These quantities also depend upon the magnitudes of the feed and cable losses and the temperature scale realized in the measurements, two system characteristics for which absolute measurements aboard an orbiting system are exceedingly difficult. Strictly, the best single means of comparing HALCA's sensitivity with ground radio telescopes is with the SEFD, as this quantity is independent of these effects; indeed, this is all that is required for planning VLBI observations. SEFD values for all GRTs likely to be involved in HALCA observations are given in Table 6.

12.2 Inter-Channel Phase Calibration

The phase stability or coherence of the radio-source wavefronts recorded at each radio telescope is crucially important to successful VLBI observations, and this is achieved by using atomic frequency and timing standards to drive the observations and by using detailed wavefront model in correlation. For HALCA, transfer of the reference phase from the tracking stations and uncertainties in the orbit determination and timing impose stricter coherence limits than is typical of ground-based VLBI. Since HALCA's complex sensitivity is relatively small in magnitude and less certain in phase, the relative coherence between its dual IF channels may be important for many observations.

In two of the three VSOP observing modes, including the mode that is VLBA/MkIV/S2 compatible, two IF channels of VLBI data are recorded. However, as is true of multi-IF ground-based VLBI, there are arbitrary delay and phase offsets between the two IF channels (due to independent electronics) which may vary slowly with time. These offsets need to be measured and removed from the VLBI data if the IF channels are to be coherently averaged to obtain the full-bandwidth sensitivity for VLBI fringe detection. As is for ground-based telescopes, two methods for calibrating HALCA's delay and phase offsets exist. First, if the offsets are thought to be constant with time (usually a good assumption in ground-based VLBI), a single short scan–during which the fringes between ground radio telescopes and HALCA are strong within each of channels separately–can be used to measure offsets that are applicable to the entire dataset. Slow and/or monotonic variations (available HALCA data has shown such variations) can be tracked by using multiple strong scans. The second method (typically less reliable than the first for ground telescopes) involves a series of phase calibration tones that are continuously injected into the LNAs at 1 MHz intervals (the sum of the power in these tones is only 0.4% of the system temperature power). The relative phases of these tones are extracted at the tracking stations and/or correlators and are currently being tested as a means of measuring the offsets between the two channels. The phase cal tones may also be useful for bandpass calibration within each channel.

The current data reduction experience suggests that only VSOP observations of the very weakest or most-resolved sources will require alignment of the IF channels for the purpose of VLBI fringe detection. Proposers expecting that this calibration will be a crucial requirement for their observation should be aware that slewing to strong calibration sources, as is typically done for ground-only VLBI, is not possible with HALCA, and that the phase calibration tone system is not yet fully tested. Should the tone system be declared reliable, the PI of an experiment will not have to worry about the extraction of these tones as this responsibility will be assumed by the VSOG, with results reported to the proposer in tables accompanying their amplitude calibration data. In any case, for continuum observations the tones will always be on and for spectral line observations they will always be off by default.

12.3 Summary

The VSOG is responsible for developing the calibration scheme for HALCA and will supply a spacecraft calibration file that contains all of the relevant information to perform reliable *a priori* calibration and flagging of the HALCA data. This file will be in a standard format so that the usual programs used for calibrating VLBI data can be used, such as the UVFLG, ANTAB, APCAL, PCLOD, and PCCOR programs in AIPS. As the detailed system temperature, antenna sensitivity, and phase calibration tone behavior are better understood, this information will be made available on the VSOP WWW site (http://www.vsop.isas.ac.jp).

Similar calibration data for ground radio telescopes will be supplied as is conventionally done with ground-only observations. Pending availability at each correlator, it is possible that all calibration information (HALCA and GRTs) will accompany the visibility data as tables attached to the FITS-format distribution.

13 VSOP Simulation Software

As has been demonstrated in several sections of this guide, VSOP observations with HALCA are quite different from ground-only VLBI. To help potential users better understand the VSOP mission and hence write better proposals, three sets of software have been written to enable proposers to plan experiments. The major difference between the three software packages is the platforms they run on and the functions they can perform. Software inter-comparisons have shown that the three sets of software give the same correct results for the functions they have in common. Table 14 compares the three software packages.

Further details on the individual packages are provided in the following subsections. It should be noted that all three packages have been updated to include the present HALCA orbit and spacecraft constraints including the solar constraints.

Table 14: Comparison of the JPL, Calgary and SGO Space VLBI Simulation Software Packages

Package Organization Country	FAKESAT JPL USA	SPAS SGO Hungary	SVPIS U. of Calgary Canada
Platform	UNIX	PC	PC
Feature			
VSOP spacecraft constraints	•	•	•
Satellite ground track	•	•	•
(u,v) plot	•	•	•
All-Sky (u,v) plot	•	•	•
(u,v) plot as a function of time	•	•	
Rotating Earth movie	•	•	
Create simulated data	•		•
Radio telescope timeline	•	•	•
SNR calculations	•	•	•
Polarization simulations			•

•= software package supports this feature
SPAS = Space VLBI Assistance Software
SVPIS = Space VLBI Principal Investigator Software
SGO = Satellite Geodetic Observatory

13.1 FAKESAT

The JPL Space VLBI Project has developed a space VLBI simulation program, called FAKESAT, that enables proposers to the space VLBI missions, VSOP and RadioAstron, plan their experiments. FAKESAT was derived from the well-established Caltech VLBI package program FAKE and has a mouse-driven, interactive point and click, X-windows interface. At present FAKESAT runs on Sun, HP, and Dec alpha workstations but it should be easy to port it to other UNIX platforms. It requires the Caltech PGPLOT library. A variety of VSOP simulations can be undertaken with FAKESAT (see Table 14).

FAKESAT is available either from the JPL SVLBI Project WWW site (http://sgra.jpl.nasa.gov) or by anonymous ftp from sgra.jpl.nasa.gov (128.149.70.4) with the relevant compressed tar and README files in the pub/software/fakesat directory.

13.2 SPAS

The Space VLBI Assistance Software (SPAS) has been developed at the FÖMI Satellite Geodetic Observatory, Penc (Hungary). Some of the main functions of the software are shown in Table 14. A graphical user interface enables the user to communicate with the software easily. Commands can be given by mouse or keyboard. Plots and tables can be printed out on various printers. The recommended hardware (IBM PC/AT compatible) configuration is the following: MS-DOS or DR-DOS V5.0, V6.0, 80486 66 MHz processor, about 3 MB free disk space, 8 MB RAM, SVGA with 1 MB VRAM graphics card, keyboard + mouse input and a HP LaserJet printer.

The new version (v2.0) and the full user documentation is available on request. SPAS can be obtained by anonymous ftp from ftp.sgo.fomi.hu (193.224.183.66) and is in the SPAS/EXE directory. For more information see `http://www.sgo.fomi.hu/vlbi/spas.htm` or contact the project leader:

I. Fejes, FÖMI Satellite Geodetic Observatory, Penc, Hungary.
Postal address: H-1373 Budapest, P.O. Box 546.
Tel.: +36 27 310 980, fax: +36 27 310 982.
E-mail: vlbi_group@novell.sgo.fomi.hu

13.3 SVPIS

Under contract to the Canadian Space Agency, the University of Calgary has developed a suite of software programs for personal computers to aid potential investigators to formulate technically sound observing proposals. The software enables a potential investigator to explore the impact of a range of observational choices on the scientific goals of the experiment. See Table 14 for what functions the software can perform.

The software runs on personal computers under Windows95 or NT with a standard windows mouse-driven Graphical User Interface. A keyboard-driven DOS version is also available. The software and user documentation can be obtained by anonymous ftp from ftp.ras.ucalgary.ca in the 'outgoing/svlbi' directory.

14 VSOP Data Analysis

14.1 Data Reduction

Now that some data from the early stages of the VSOP mission have already been reduced, documentation for the various data reduction packages which describe techniques for the analysis of space VLBI data are available. In general, fringe fitting of VSOP correlated data is performed using fringe-fitting tasks within NRAO's Astronomical Image Processing System (AIPS) and imaging is done either in AIPS or in the Caltech Difmap package.

A new AIPS CookBook chapter on VLBI data reduction, including the reduction of VSOP data is now available at the following URL:

http://www.nrao.edu/~kdesai/files/COOK910.ps

The Difmap documentation has also been revised to include a section on imaging space VLBI data. This documentation can obtained at the following URL:

ftp://astro.caltech.edu/pub/difmap/cookbook.ps.Z

In addition, a VSOP Data Reduction (VDR) email distribution and exploder has been set up to facilitate discussion of data reduction issues as they arise. To subscribe to the VDR, maintained at NRAO, send e-mail to:

Majordomo@zia.aoc.nrao.edu

With the text "subscribe vdr" in the body of your e-mail message. An archive is of VDR postings is at the following URL:

http://sgra.jpl.nasa.gov/comic/vdr/VDR_update.html

For the latest information on VSOP data reduction please consult the following URL:

http://www.vsop.isas.ac.jp/obs/Reduction.html

14.2 User Support Facilities

There are also several user support facilities around the world where VSOP PIs can obtain help in the analysis of their VSOP experiments. These facilities are described by country or geographic region.

Australia

The Australia Telescope National Facility (ATNF, a division of the Commonwealth Scientific and Industrial Research Organisation, CSIRO), provides regional support for VSOP users based in, or visiting, Australia and the Asia-Pacific region. An E-mail VSOP help-desk (vlbi@atnf.csiro.au) will be supported up to and beyond the cut-off date for submission of proposals in the second AO (May 1998). The ATNF supports reduction and analysis of radio astronomical data at its headquarters at Marsfield, Sydney, through its support scientists and extensive computing facilities. VLBI observations with VSOP and with the Australian Long Baseline Array (LBA) are included in this support. The local computing system is comprised principally of Sun Ultra and Sparc machines, offering the major packages AIPS and Miriad, as well as the more specialised VLBI tools such as Difmap.

Canada

Two sites in Canada provide user support for the VSOP mission. The DRAO correlator site at Penticton British Columbia provides consulting to scientists regarding correlator signal processing capabilities to meet specific science requirements. The regional data reduction center at the University of Calgary provides support to scientists regarding data reduction, calibration, and imaging. If desired, PIs may visit the correlator site prior to or during correlation if specific science requirements warrant one-on-one interaction with correlator personnel. Also, PIs may visit the University of Calgary to get assistance with data reduction and imaging.

Europe/China

The Joint Institute for VLBI in Europe (JIVE, Dwingeloo, The Netherlands) provides regional support for VSOP users affiliated with European and Chinese institutes. JIVE operates a VSOP Help Desk (see §15) during the AO2 proposal preparation period (through 08 May 1998). JIVE support scientists will be available to assist VSOP users at all stages of their VSOP experiments (proposing – scheduling – data reduction). A network of Sun Ultra workstations is available at JIVE for VLBI data reduction and analysis. In particular, an Sun Ultra-10 with 256 Mbytes of physical memory and 13 Gbytes of disk space is dedicated to VSOP data reduction.

Japan

Both the Institute of Space and Astronautical Science (Sagamihara) and the National Astronomical Observatory (Mitaka) are able to support users with assistance from the proposal preparation through to the data reduction. Dedicated computing facilities are available at both locations for fringe-fitting and imaging VSOP data.

United States

The regional user support facility for VSOP PIs based at US institutions is operated by NRAO at the Array Operations Center in Socorro, NM. It includes both expert personnel and high-performance computer hardware. Two scientific staff members supported by NASA, and a third by JIVE, have developed substantial expertise in areas of data analysis specialized for Space VLBI: fringe fitting, calibration, and imaging. A Silicon Graphics Origin 200 compute server and two model O2 visualization workstations are available on the standard AOC sign-up basis for analysis of VSOP observations."

15 VSOP Proposal Help

Regional assistance for prospective proposers is available from a number of different sites. Questions relating to the AO, proposal submission, technical aspects of the VSOP mission, or proposal aid software that are not answered elsewhere in this Proposer's Guide or the AO, may addressed via e-mail to these sites. Such questions will also be compiled to create a "Frequently Asked Questions" file, which can be inspected using the World Wide Web (URL: http//www.vsop.isas.ac.jp/), or obtained using anonymous ftp from www.vsop.isas.ac.jp (133.74.2.131). Please refer to this file before contacting the e-mail addresses listed in Table 15.

Table 15: E-mail Addresses for Regional Help (until 8 May 1998)

Region	e-mail contact
Australasia/Africa	vsop_help@atnf.csiro.au
Canada	vsop_help@ras.ucalgary.ca
CIS	vsop_help@dpc.asc.rssi.ru
Europe/China	vsop_help@jive.nfra.nl
Japan	vsop_help@vsop.isas.ac.jp
USA	vsop_help@sgra.jpl.nasa.gov
Elsewhere	vsop_help@vsop.isas.ac.jp

Questions directed to the regional experts will be responded to in a timely manner. As the resources for proposal support are limited, however, questions should be asked as early in the proposal period as possible to avoid any possible congestion during the last weeks before the deadline. These e-mail addresses will be valid until the second AO deadline.

16 Web Sites for Additional Information

The prime web site for all VSOP related material is the VSOP web site at ISAS:

http://www.vsop.isas.ac.jp

There are also secondary VSOP web sites that provide more information on specific mission elements. These sites, along with the VSOP site at ISAS, are listed in Table 16.

Table 16: VSOP Related Web Sites

Web Site	URL
VSOP Project (ISAS)	http://www.vsop.isas.ac.jp
VSOP Mitaka Group	http://hotaka.mtk.nao.ac.jp/index-e.html
NRAO Space VLBI Project	http://www.nrao.edu/~julvesta/aoc_svlbi.html
NRAO Green Bank OVLBI Station	http://info.gb.nrao.edu/ovlbi/OVLBI.html
US Space VLBI Project (JPL)	http://sgra.jpl.nasa.gov/
Joint Institute for VLBI in Europe (JIVE)	http://www.nfra.nl/jive
Space VLBI at DRAO (Canadian correlator)	http://www.drao.nrc.ca/web/vlbi/spacevlbi.html
University of Calgary	http://www.ras.ucalgary.ca/Spacevlbi.html

17 Acknowledgments

B. Carlson, P. Edwards, S. Frey, D. Meier, G. Moellenbrock, D. Murphy, J. Romney, R. Taylor and S. Tingay provided material for the revised version of the Proposer's Guide released in conjunction with the second VSOP AO. The original version of the Proposer's Guide included contributions from D. Murphy, P. Edwards, D. Gabuzda, H. Hirabayashi, M. Inoue, H. Kobayashi, D. Meier, G. Moellenbrock, Y. Murata, I. Noszticzius, R. Taylor, J. Ulvestad and A. Wiercigroch.

This version of the Proposer's Guide has been improved with comments on earlier drafts from L. Gurvits, H. Kobayashi, A. Mioduszewski, and R. Preston.